Article

Cell Stem Cell

GFAP Mutations in Astrocytes Impair Oligodendrocyte Progenitor Proliferation and Myelination in an hiPSC Model of Alexander Disease

Graphical Abstract

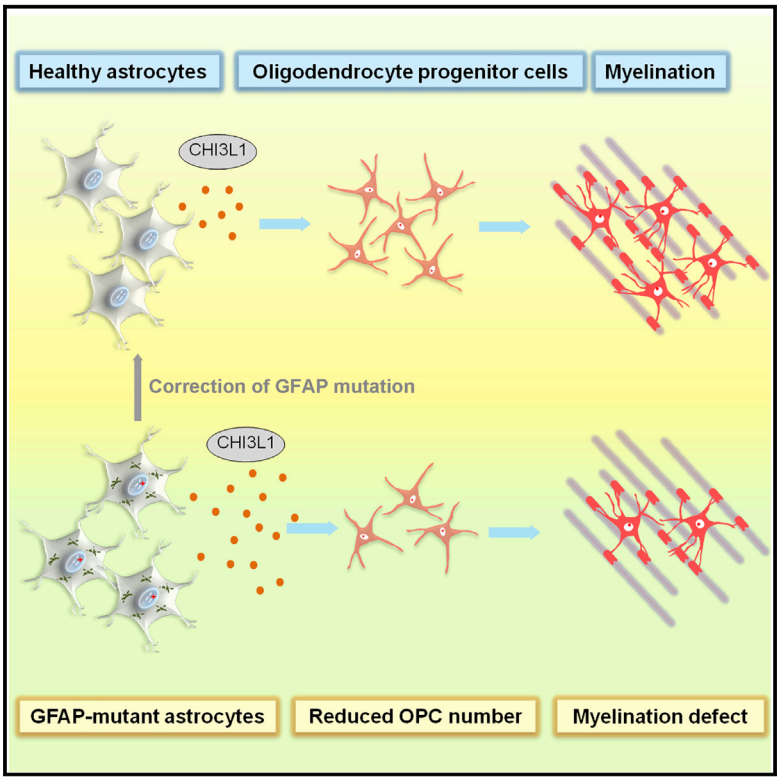

Authors

Li Li, E Tian, Xianwei Chen, ..., Neville E. Sanjana, Arthur D. Riggs, Yanhong Shi

Correspondence

yshi@coh.org

In Brief

Shi and colleagues used Alexander disease (AxD) patient iPSC-derived astrocytes to recapitulate AxD patient phenotypes that could not be achieved in animal models and uncover molecular mechanisms underlying myelination defect in the disease. They found that disease astrocytes secret molecules to inhibit oligodendrocyte progenitor cell function and impair myelination.

Highlights

- Human iPSC-derived glial cells recapitulate leukodystrophic myelination defects
- AxD patient iPSC-derived astrocytes exhibit GFAP aggregates and Rosenthal fibers
- AxD astrocytes inhibit OPC proliferation and myelination
- GFAP mutant human astrocytes secrete CHI3L1 to inhibit human OPC function

Li et al., 2018, Cell Stem Cell *23*, 239–251
August 2, 2018
https://doi.org/10.1016/j.stem.2018.07.009

CellPress

Cell Stem Cell
Article

GFAP Mutations in Astrocytes Impair Oligodendrocyte Progenitor Proliferation and Myelination in an hiPSC Model of Alexander Disease

Li Li,[1,2,9] E Tian,[1,9] Xianwei Chen,[1] Jianfei Chao,[1] Jeremy Klein,[1] Qiuhao Qu,[1] Guihua Sun,[3] Guoqiang Sun,[1] Yanzhou Huang,[1] Charles D. Warden,[4] Peng Ye,[1] Lizhao Feng,[1] Xinqiang Li,[1] Qi Cui,[1] Abdullah Sultan,[1] Panagiotis Douvaras,[5] Valentina Fossati,[5] Neville E. Sanjana,[6,7,8] Arthur D. Riggs,[3] and Yanhong Shi[1,2,10,*]

[1]Division of Stem Cell Biology Research, Department of Developmental and Stem Cell Biology, Beckman Research Institute of City of Hope, Duarte, CA 91010, USA
[2]Irell and Manella Graduate School of Biological Sciences, Beckman Research Institute of City of Hope, Duarte, CA 91010, USA
[3]Department of Diabetes Complications and Metabolism, Diabetes and Metabolism Research Institute, Beckman Research Institute of City of Hope, Duarte, CA 91010, USA
[4]Integrative Genomics Core, Beckman Research Institute of City of Hope, Duarte, CA 91010, USA
[5]The New York Stem Cell Foundation Research Institute, New York, NY 10019, USA
[6]New York Genome Center, New York, NY 10013, USA
[7]Department of Biology, New York University, New York, NY 10003, USA
[8]Massachusetts Institute of Technology, Cambridge, MA 02142, USA
[9]These authors contributed equally
[10]Lead Contact
*Correspondence: yshi@coh.org
https://doi.org/10.1016/j.stem.2018.07.009

SUMMARY

Alexander disease (AxD) is a leukodystrophy that primarily affects astrocytes and is caused by mutations in the astrocytic filament gene *GFAP*. While astrocytes are thought to have important roles in controlling myelination, AxD animal models do not recapitulate critical myelination phenotypes and it is therefore not clear how AxD astrocytes contribute to leukodystrophy. Here, we show that AxD patient iPSC-derived astrocytes recapitulate key features of AxD pathology such as GFAP aggregation. Moreover, AxD astrocytes inhibit proliferation of human iPSC-derived oligodendrocyte progenitor cells (OPCs) in co-culture and reduce their myelination potential. CRISPR/Cas9-based correction of GFAP mutations reversed these phenotypes. Transcriptomic analyses of AxD astrocytes and postmortem brains identified CHI3L1 as a key mediator of AxD astrocyte-induced inhibition of OPC activity. Thus, this iPSC-based model of AxD not only recapitulates patient phenotypes not observed in animal models, but also reveals mechanisms underlying disease pathology and provides a platform for assessing therapeutic interventions.

INTRODUCTION

Astrocytes are the most abundant type of glial cells in the mammalian central nervous system (CNS). The important functions for astrocytes in neurodevelopment and diseases have been increasingly appreciated because of their key roles in maintaining CNS homeostasis and close interactions with other cell types in the brain (Verkhratsky and Parpura, 2016). Astrocytes are critical for neuronal maturation, synapse formation, and survival (Molofsky et al., 2012; Clarke and Barres, 2013; Allen and Eroglu, 2017). They are also an integral part of the blood-brain barrier (Abbott et al., 2006) and neuroinflammation in the brain (Colombo and Farina, 2016). Growing evidence supports the idea that astrocytes play an important role in regulating myelination (Sofroniew and Vinters, 2010; Lanciotti et al., 2013; Domingues et al., 2016; Kıray et al., 2016). Oligodendrocytes are the myelinating glia of the CNS derived from oligodendrocyte progenitor cells (OPCs) (Domingues et al., 2016). The interplay between astrocytes and OPCs could modulate oligodendrocyte homeostasis and myelination.

Alexander disease (AxD) is a type of leukodystrophy that primarily affects astrocytes (Messing et al., 2010). It represents the first example of neurological diseases with astrocyte dysfunction as the primary cause (Messing et al., 2012; Lanciotti et al., 2013). AxD is due to mutations in glial fibrillary acidic protein (GFAP), the major intermediate filament protein in astrocytes, resulting in the formation of protein aggregates known as Rosenthal fibers (Iwaki et al., 1989; Johnson and Bettica, 1989). These fibers accumulate within the astrocyte cytoplasm, causing cellular dysfunction with devastating effects on CNS, including OPC and oligodendrocyte loss and demyelination in AxD patients (Prust et al., 2011).

Although multiple animal models have been established to study AxD and contributed to our knowledge of AxD substantially, none of these models exhibit myelination defect (Messing et al., 1998; Hagemann et al., 2005, 2006; Tanaka et al., 2007b; Wang et al., 2011, 2015; Lee et al., 2017), an important pathological phenotype in AxD patients, especially the most

common, early-onset patients (Messing et al., 2001; van der Knaap et al., 2001). This is likely due to differences between human astrocytes and astrocytes of other species: human astrocytes are much larger and more complex and therefore may contribute to disease progression to a greater extent than astrocytes in rodents and other non-human species (Verkhratsky et al., 2012). In this study, we sought to establish a human cellular model of AxD to uncover the mechanisms of AxD pathology that are not recapitulated in animal models.

Human induced pluripotent stem cells (hiPSCs) provide a valuable tool to study human genetic disorders (Takahashi et al., 2007; Yu et al., 2007), especially neurological diseases, for which human cells and tissues are not easily accessible (Marchetto et al., 2011; Li et al., 2018; Shi et al., 2017). hiPSCs can retain mutations of relevant patients and be differentiated into cell type(s) that are dysfunctional in the disease of interest, thus allowing identification of pathological mechanisms underlying the disease by comparison of patient and healthy control (HC) iPSC-derived cells through functional assays, cellular analyses, and molecular profiling. Modeling AxD using hiPSCs could allow us to close the knowledge gap between findings from animal models and patient phenotypes.

In hiPSC-based disease modeling, iPSCs derived from healthy individuals are usually used as controls for patient-derived iPSCs. With rapid development of genome editing technologies, the generation of isogenic iPSC lines with the edited gene as the sole variable allows for identification of true pathological phenotypes, without worrying about changes resulting from different genetic or epigenetic backgrounds (Hockemeyer and Jaenisch, 2016). Studying AxD pathogenesis using isogenic iPSC-derived astrocytes with the *GFAP* mutation as the sole variant would enable us to identify pathological phenotypes explicitly caused by the *GFAP* mutation.

In this study, we generated iPSCs from HC individuals and AxD patients, and isogenic iPSCs that have the mutant *GFAP* in AxD iPSCs corrected to the wild-type (WT) genotype through CRISPR/Cas9-based gene editing. We differentiated both control and AxD iPSCs into astrocytes and established an astrocyte-OPC co-culture system using these astrocytes together with HC iPSC-derived OPCs. We used the co-culture system and a nanofiber-based *in vitro* myelination assay to determine how AxD astrocytes regulate oligodendroglial lineage cell number to modulate myelination, and performed transcriptome analysis to identify molecular mechanisms underlying this regulation.

RESULTS

GFAP Mutant AxD iPSCs Can Be Differentiated into Astrocytes

To study the pathological effects of AxD *GFAP* mutations in a human cellular model, we generated hiPSCs from fibroblasts of three HC individuals (C1, C3, and I90) and three AxD patients (Figure 1A) through episomal reprogramming (Wen et al., 2014; Kime et al., 2015). Among the three AxD patients, two carry hotspot *GFAP* mutations at either Arg (R) 79 or R239 (Hagemann et al., 2006), including an R79C (AxD997) and an R239C mutation (AxD825), and another has an M73K mutation (AxD999) in the *GFAP* coding region (Figure 1B). To identify true *GFAP* mutation-relevant phenotypes independent of line-to-line variation, we generated isogenic iPSCs by correcting the *GFAP* mutation site (M73K) in AxD999 iPSCs using the CRISPR/Cas9 nickase (Ran et al., 2013a) (Figures 1C, S1E, and S1F). Correction of the M73K mutation site in the selected clone was confirmed by Sanger sequencing of the *GFAP* gene (Figure 1C). This CRISPR/Cas9-edited AxD999 clone containing the WT *GFAP* gene was termed AxD999-CR. No off-target effect was detected in the AxD999-CR iPSCs during CRISPR/Cas9 editing (Table S6). All iPSC lines were characterized for pluripotency and normal karyotype (Figure S1) and authenticated by short tandem repeat (STR) assay (Table S1).

Because GFAP is predominantly expressed in astrocytes, to investigate the effect of the AxD *GFAP* mutations on astrocyte function, we differentiated control and AxD iPSCs into astrocytes. To achieve consistency in astrocyte purity across lines, we transduced the iPSC-derived astrocytes with lentivirus encoding the human GFAP-promoter-driven-GFP (GFAP-GFP) reporter. Human primary astrocytes and fibroblasts were included as the positive and negative control, respectively (Figures S2A–S2C). We sorted the GFAP-GFP-positive iPSC-derived astrocytes by fluorescence-activated cell sorting (FACS) (Figure S2D). The sorted astrocytes expressed the astrocyte markers GFAP and S100β (Figures 1D–1F). The purity of the sorted astrocytes is consistent across all lines based on the percentage of the $GFAP^+$ cells and the $S100\beta^+$ cells after sorting (Figures 1D and 1E). The hiPSC-derived astrocytes expressed other astrocyte markers, such as SOX9 (Figure S2E) (Zhang et al., 2016), CD44, GLUL, and SCL1A3 as well (Table S2). These astrocytes also expressed many mature astrocyte markers described in published studies (Hasel et al., 2017; Sloan et al., 2017) (Table S3).

The iPSC-derived astrocytes were not contaminated by oligodendrocyte lineage cells, neurons, endothelial cells, and fibroblasts, as revealed by negative staining of the oligodendrocyte lineage markers, OLIG2, O4, and MBP, and the other lineage-specific markers, MAP2, CD31, and FSP (Figure S3A). These astrocytes could survive and express the human astrocytic marker hGFAP after transplanting into mouse brains (Figure S3B), generate Ca^{2+} flux in response to ATP (Figure S3C), and display a transient voltage-dependent outward current followed by a sustained lower current (Figure S3D), similar to the pattern of astrocytes shown previously (Krencik et al., 2011). These astrocytes were used for the following studies.

AxD Astrocytes Exhibit Rosenthal Fiber-like Structure

GFAP immunostaining revealed that the AxD astrocytes displayed patches of GFAP filament bundles or aggregates in the cytoplasm, in contrast to control astrocytes, in which the GFAP filaments are distributed evenly in the cytoplasm (Figures 1F and 1G). This observation was confirmed by electron microscopy (EM) analysis, which revealed dense aggregation of filaments in AxD astrocytes, resembling early Rosenthal fiber structure (Figure 1H). In contrast, the AxD999-CR astrocytes didn't exhibit bundles of GFAP filaments as revealed by both immunostaining (Figure 1G) and EM analyses (Figure 1H), in a manner similar to HC astrocytes. Because Rosenthal fibers are mostly composed of GFAP and the small heat shock proteins αB-crystallin (Tomokane et al., 1991), to confirm the

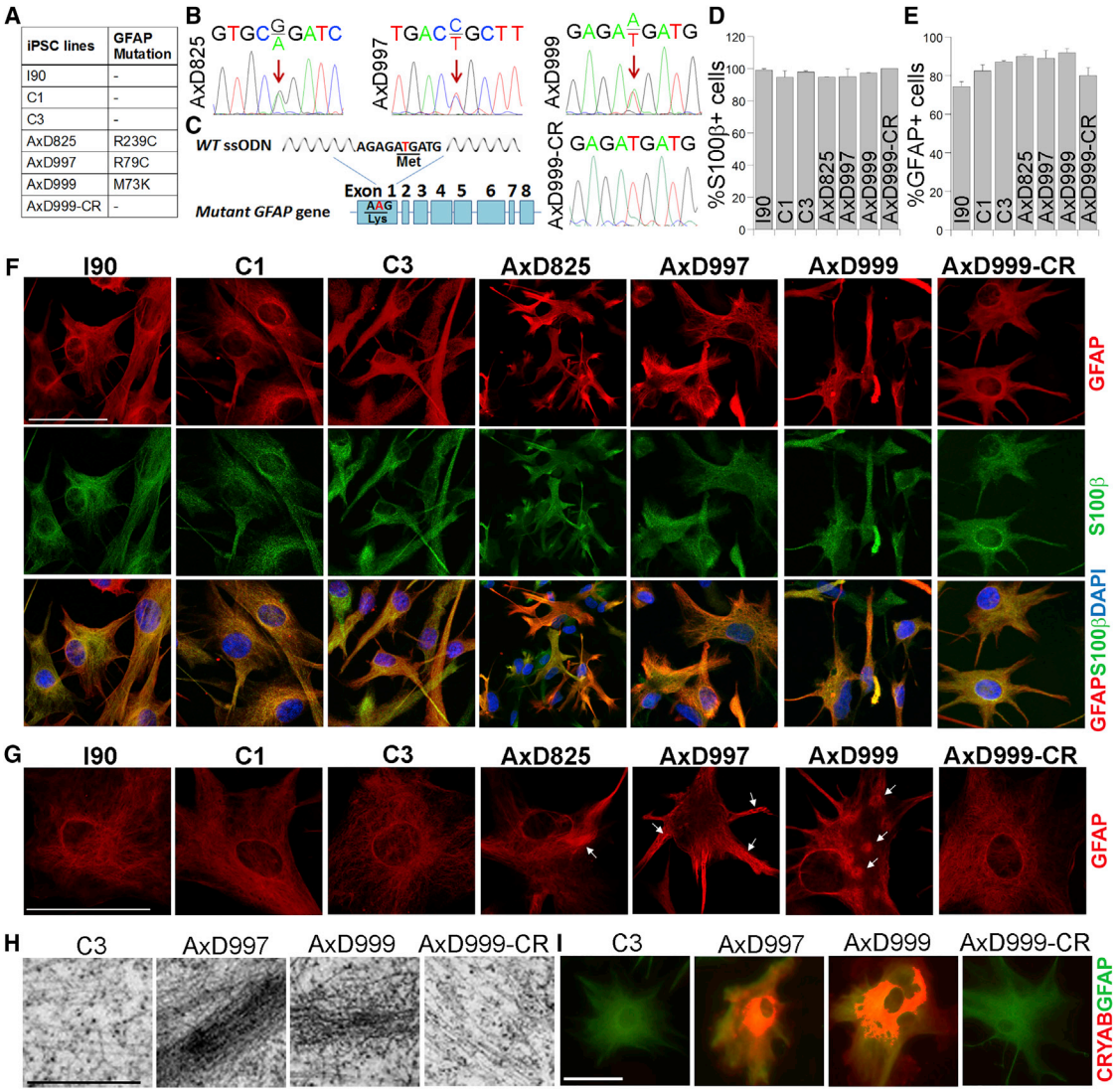

Figure 1. AxD Patient iPSC-Derived Astrocytes Exhibit GFAP Aggregates

(A) hiPSC lines used in the study, including three control lines, I90, C1, and C3; three AxD lines, AxD825, AxD997, and AxD999; and an isogenic line, AxD999-CR, with the *GFAP* mutation corrected by CRISPR/Cas9 editing.

(B) *GFAP* mutations in AxD iPSC lines shown by sequencing.

(C) Schematic for CRISPR/Cas9 targeting of the *GFAP* mutation (M73K) in AxD999 iPSCs, and sequence confirming the WT genotype of AxD999-CR iPSCs.

(D–F) The percentage of S100 β^+ (D) and GFAP$^+$ (E) cells, and representative images of GFAP and S100 β staining (F) in iPSC-derived astrocytes. Error bars are SD of the mean; n = 3 experimental repeats for (D) and (E).

(G) Representative images of GFAP aggregates (pointed by white arrows) in AxD iPSC-derived astrocytes shown by immunostaining. The GFAP aggregates were absent in control and AxD999-CR astrocytes.

(H) EM images of filament bundles resembling Rosenthal fibers in AxD997 and AxD999 astrocytes, but not C3 and AxD999-CR astrocytes. n = 4 experimental repeats.

(I) Representative images of GFAP and αB-Crystalline (CRYAB) double staining in AxD997 and AxD999 astrocytes. No αB-Crystalline signal was detected in C3 and AxD999-CR astrocytes.

Scale bar, 50 μm for (F), (G), and (I); 0.5 μm for (H). See also Figures S1–S3 and Tables S1–S3, S5, and S7.

presence of Rosenthal fibers in AxD astrocytes, we immunostained the AxD astrocytes for GFAP and αB-crystallin. Consistent with the EM analysis, we observed GFAP and αB-crystallin double-positive signal in AxD astrocytes, but not in control astrocytes (C3 or AxD999-CR) that have the WT *GFAP* gene (Figure 1I). These results indicate that the AxD iPSC-derived astrocytes exhibit structural differences in GFAP filaments from control iPSC-derived astrocytes, and that the Rosenthal fiber-like structure in AxD999 astrocytes was caused by *GFAP* mutation, because no such structure was detected in the isogenic AxD999-CR astrocytes that have the *GFAP* mutation corrected.

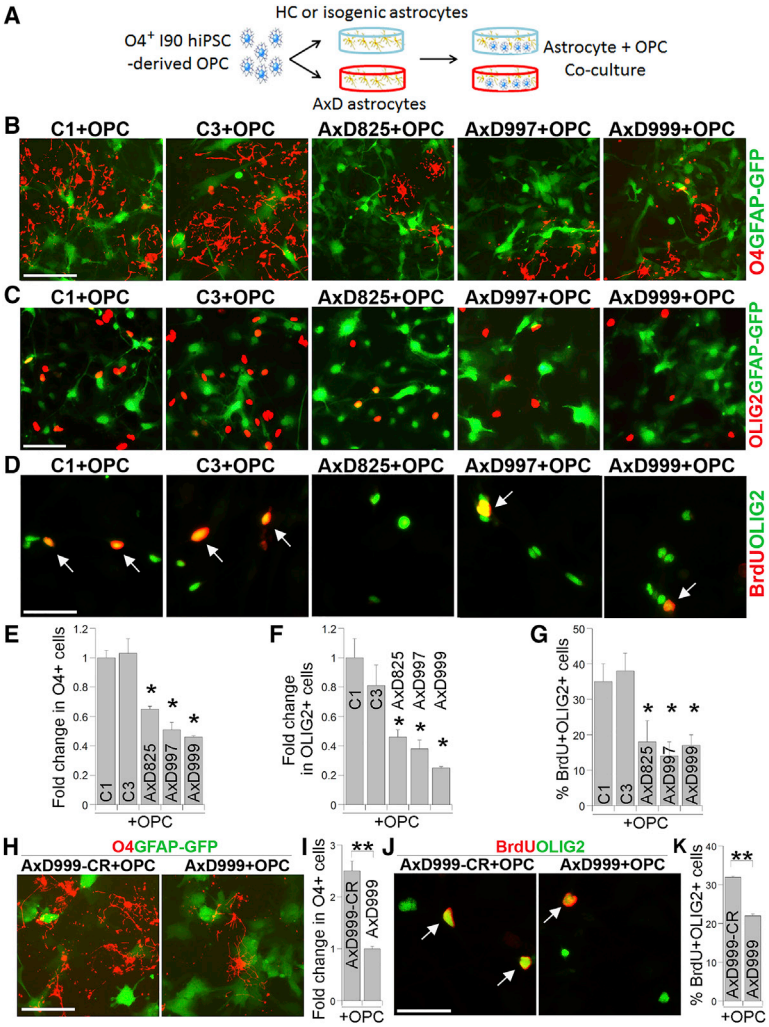

Figure 2. AxD Astrocytes Reduce OPC Proliferation

(A) Schematic of OPC-astrocyte co-culture system. O4-sorted I90 iPSC-derived OPCs were seeded onto GFAP-GFP-sorted control or AxD astrocytes for co-culture.

(B and E) Representative images of O4 live staining (B) and fold change in $O4^+$ cell number (E) after 5-day co-culture of OPCs with control or AxD astrocytes.

(C and F) Representative images of OLIG2 staining (C) and fold change in $OLIG2^+$ cell number (F) after 5-day co-culture.

(D and G) Representative images of BrdU and OLIG2 double staining (D) and the percentage of $BrdU^+OLIG2^+$ cells (E) after 24 hr co-culture.

(H and I) Representative images of O4 live staining (H) and fold change in $O4^+$ cell number (I) after 5-day co-culture of OPCs with AxD999-CR or AxD999 astrocytes.

(J and K) Representative images of BrdU and OLIG2 double staining (J) and the percentage of $BrdU^+OLIG2^+$ cells (K) after 24 hr co-culture of OPCs with AxD999-CR or AxD999 astrocytes. Arrows point to the $BrdU^+OLIG2^+$ cells.

Scale bar, 100 μm for (B), (D), and (H); 50 μm for (C) and (J). Error bars are SE of the means; n = 3 experimental repeats; *$p < 0.05$ by one-way ANOVA for (E)–(G), **$p < 0.01$ by Student's t test for (I) and (K). See also Figure S4.

AxD Astrocytes Reduce OPC Proliferation

Because AxD is caused by mutation of the astrocytic gene *GFAP*, and myelination defect is the major pathological phenotype in AxD patients (Messing et al., 2012), we hypothesized that AxD astrocytes could cause myelination defects through interaction with oligodendroglial lineage cells. To test this hypothesis, we established a co-culture system consisted of hiPSC-derived astrocytes and OPCs. Human HC iPSCs were differentiated into $OLIG2^+$ and $NKX2.2^+$ pre-OPCs, followed by induction into $O4^+$ OPCs (Douvaras and Fossati, 2015). The $O4^+$ OPCs were further matured into myelinating oligodendrocytes that expressed the mature oligodendrocyte marker myelin basic protein (MBP) (Figure S4A). We set up the co-culture system by incubating the GFAP-GFP-sorted control or AxD astrocytes with the O4-sorted HC iPSC-derived OPCs (Figure 2A). The sorted OPCs expressed the OPC markers O4 and OLIG2, but not the mature oligodendrocyte marker MBP (Figures S4B and S4C). Notably, we observed a significant decrease in the number of $O4^+$ OPCs after 5-day co-culture of OPCs with AxD astrocytes, compared to co-culture with control astrocytes (Figures 2B and 2E). This observation was confirmed in a co-culture assay, in which the number of oligodendroglial lineage cells was evaluated by immunostaining with OLIG2 (Figures 2C and 2F). These results indicate that the AxD astrocytes could reduce the number of co-cultured OPCs.

To test whether the decrease in the number of OPCs co-cultured with AxD astrocytes was due to a decrease of cell proliferation or an increase of cell death, apoptosis of OPCs in the co-culture system was examined by double staining for OLIG2 and cleaved Caspase-3, a marker of apoptosis. We could barely detect any Caspase-3^+ $OLIG2^+$ cells in any co-culture group (Figures S4D and S4E), indicating that the reduced cell number in OPCs is likely not resulting from increased OPC apoptosis. We next examined the rate of OPC proliferation in the co-culture system. On day 2 of co-culture, cells were treated with BrdU. We observed a significant decrease in the percentage of $BrdU^+OLIG2^+$ OPCs when co-cultured with AxD astrocytes, compared to that when co-cultured with control astrocytes (Figures 2D and 2G). In contrast, no difference in BrdU labeling was detected between control and AxD astrocytes (Figures S4F and S4G).

To determine whether the defects in OPC proliferation were caused by *GFAP* mutation in the co-cultured AxD astrocytes, we compared the OPC proliferation rate between AxD999 and AxD999-CR co-cultures. The number of OPCs significantly decreased in co-culture with AxD999 astrocytes, compared to that in co-culture with AxD999-CR astrocytes, as revealed by O4 staining (Figures 2H and 2I). Accordingly, we observed a substantial decrease in OPC proliferation rate in co-culture with AxD999 astrocytes, compared to that in co-culture with AxD999-CR astrocytes, as revealed by BrdU and OLIG2 double staining (Figures 2J and 2K). In summary, hiPSC-derived astrocyte and OPC co-culture allowed us to study the effects of AxD astrocytes on oligodendrocyte lineage cells. The results from this modeling system demonstrate that AxD astrocytes could reduce the number of co-cultured OPCs through inhibiting OPC proliferation.

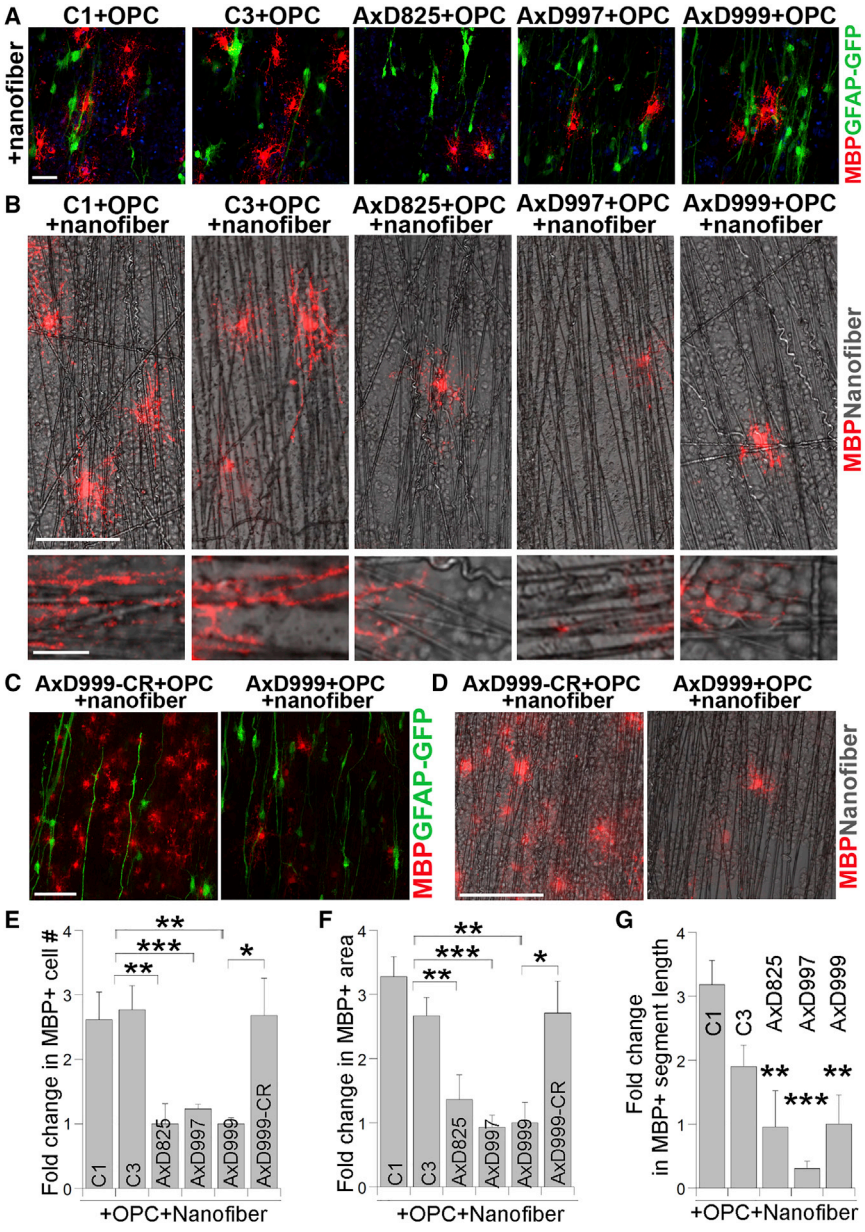

Figure 3. AxD Astrocytes Cause Myelination Defect in a 3D Nanofiber Culture System

(A and C) Representative images of MBP immunostaining in a 3D nanofiber culture system, including GFAP-GFP-sorted control versus AxD (A), or AxD999-CR versus AxD999 (C) astrocytes (green) and oligodendrocytes matured from I90 hiPSC-derived OPCs. Scale bar, 50 μm.

(B and D) Representative images of MBP immunostaining and alignment with nanofibers in control versus AxD (B), or AxD999-CR versus AxD999 (D) co-cultures. Scale bar, 100 μm. Higher magnification images are shown underneath (B) to highlight the alignment of the MBP segments with nanofibers. Scale bar, 20 μm.

(E–G) Fold change in MBP$^+$ cell number (#) (E), MBP$^+$ area (F), and MBP$^+$ segment length (G) in nanofiber-based co-culture of OPCs with astrocytes.

Error bars are SE of the means; n = 3 experimental repeats; *p < 0.05, **p < 0.01, and ***p < 0.001 by one-way ANOVA for (E)–(G). See also Figure S3.

AxD Astrocytes Induce Myelination Defect in a 3D Nanofiber Culture System

Because OPCs are the precursors of myelinating oligodendrocytes, our observation that AxD astrocytes induce decreased OPC proliferation and reduced OPC cell number prompted us to test if AxD astrocytes could induce myelination defects. To focus on the effect of astrocytes on myelination, without worrying about any potential effect from neurons, we co-cultured OPCs and astrocytes on a neuron-free, 3D nanofiber scaffold for myelin wrapping (Lee et al., 2012; Ehrlich et al., 2017). Remarkably, we found a substantially decreased number of MBP$^+$ oligodendrocytes and dramatically reduced area of MBP-covered nanofibers in the co-culture with AxD astrocytes, compared to that in the co-culture with control astrocytes (Figures 3A, 3B, 3E, and 3F). We further evaluated the wrapping of the MBP$^+$ process along the nanofibers and observed substantially decreased length of the MBP$^+$ nanofiber segments in the co-culture with AxD astrocytes (Figures 3B and 3G). Collectively, these results demonstrate that the AxD astrocytes could induce a decreased number of MBP$^+$ oligodendrocytes and reduced area of MBP-covered nanofibers, mimicking reduced area of myelination.

To evaluate the impact of astrocytic *GFAP* mutation on myelination, we co-cultured OPCs with AxD999 or AxD999-CR astrocytes on 3D nanofibers. The number of MBP$^+$ cells and the area of MBP-covered nanofibers (Figures 3C–3F and S5A) decreased substantially in the AxD999 co-culture, compared to that in the AxD999-CR co-culture. The reduced MBP-covered area is presumably due to a decreased number of MBP$^+$ cells because individual oligodendrocytes seemed to myelinate similarly when co-cultured with AxD999 or AxD999-CR astrocytes (Figure S5B). These results together indicate that the defects of OPC proliferation and myelination in the co-culture are caused by *GFAP* mutation in the AxD astrocytes.

AxD Astrocytes Exhibit Elevated Expression of Genes Associated with Cytokine Activity and Cell Membrane

Because the myelination defect could not be recapitulated in AxD animal models, the molecular and cellular mechanisms underlying the AxD pathology remain poorly understood. To identify key molecules that regulate the pathology of AxD, we performed RNA sequencing (RNA-seq) using mRNAs isolated from HC or AxD iPSC-derived astrocytes. We sorted control and AxD astrocytes by GFAP-based FACS using a method for

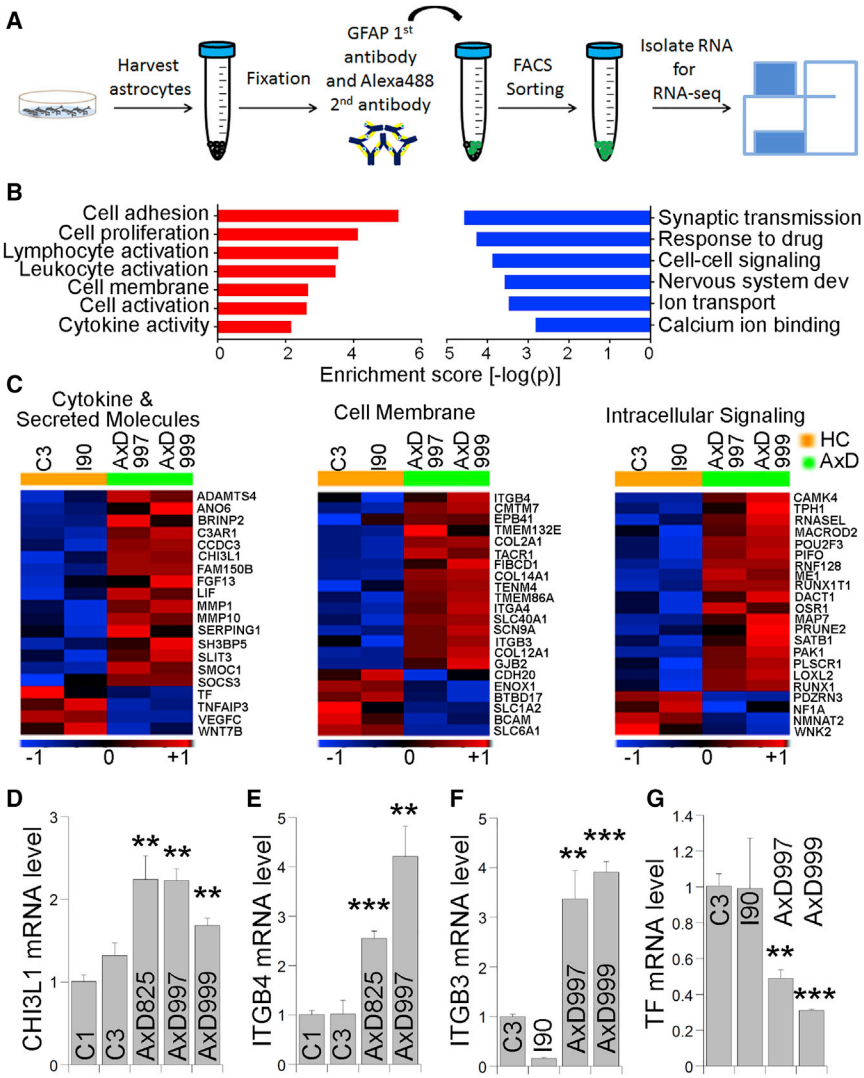

Figure 4. Transcriptome Analysis Reveals Difference between AxD and HC Astrocytes

(A) Schematic of RNA isolation from GFAP-purified astrocytes. Astrocytes were stained with GFAP antibody and the GFAP$^+$ cells were sorted by FACS, followed by RNA isolation.

(B) GO terms of genes upregulated (red) or downregulated (blue) in AxD997 and AxD999 astrocytes, compared to C3 and I90 control astrocytes. x axis is enrichment score calculated as –log (p value). Full names of abbreviated GO terms are negative regulation of cell proliferation (Cell proliferation), intrinsic component of membrane (Cell membrane), and nervous system development (Nervous system dev).

(C) Heatmap presentation of three categories of representative gene sets upregulated (red) or downregulated (blue) in AxD astrocytes compared to control astrocytes, including genes encoding cytokines and secreted molecules, cell membrane proteins, and proteins involved in intracellular signaling.

(D–G) qRT-PCR validation of *CHI3L1* (D), *ITGB4* (E), *ITGB3* (F), and *TF* (G) mRNA levels in control and AxD astrocytes.

Error bars are SD of the mean; n = 3 experimental repeats; **p < 0.01 and ***p < 0.001 by Student's t test, compared to C1 (D and E) or C3 (F and G).

analyzing RNA following intracellular sorting (MARIS) (Hrvatin et al., 2014) and isolated mRNA from the sorted cells (Figure 4A).

Comparing the transcriptome of AxD and control astrocytes revealed a set of differentially expressed genes between the two groups, including 128 significantly upregulated and 104 significantly downregulated genes in AxD astrocytes. Gene Ontology (GO) analysis revealed that genes significantly upregulated in AxD astrocytes are involved in cell adhesion, cell membrane composition, immune cell activation, and cytokine activity, whereas genes significantly downregulated in AxD astrocytes are involved in supportive functions of astrocytes, such as synaptic transmission and ion transport (Figure 4B). We selected three main categories of functions and listed 20–22 representative genes that have |fold-change| > 1.5 in each category, including cytokine and secreted factors, cell membrane components and receptors, and intracellular signaling molecules (Figure 4C). We validated a subset of these genes by qRT-PCR. Upregulation of *CHI3L1*, *ITGB4*, and *ITGB3*, and downregulation of *TF* in AxD astrocytes, compared to control astrocytes, was confirmed by qRT-PCR (Figures 4D–4G). These results together indicate that AxD astrocytes exhibit a substantially different gene expression profile from control astrocytes, and this difference could contribute to the pathological phenotypes observed in AxD.

AxD Patient Brains Exhibit Increased Expression of *CHI3L1*

To determine if the change in gene expression identified in AxD iPSC-derived astrocytes also occurs in AxD patient brains, we obtained AxD patient brain tissues along with age-matched non-AxD control brain tissues from NIH Neurobiobank (Figure S6A). All brain tissues were from the frontal lobe cortex because the frontal lobe is the predominant region with white matter abnormalities in AxD patients (van der Knaap et al., 2001; van der Voorn et al., 2009). Characteristic Rosenthal fiber structures could be detected in the AxD patient brains, but not in the non-AxD control brains (Figure S6B). RNA-seq analysis identified genes that were differentially expressed between control and AxD brains (Figure 5A). Compared to the control brains, 2,304 genes were upregulated and 1,107 genes downregulated in the AxD brains.

A number of genes showed the same trend of expression change in AxD brains as that in AxD astrocytes (Figure 5B; Table S4). GO term analysis revealed that immune response, cytokine production, and cell membrane-related biology were among the functions associated with genes upregulated in both AxD astrocytes and brains, whereas neural development-related processes, including axon ensheathment and myelination, were associated with genes downregulated in both AxD astrocytes and brains (Figure 5C).

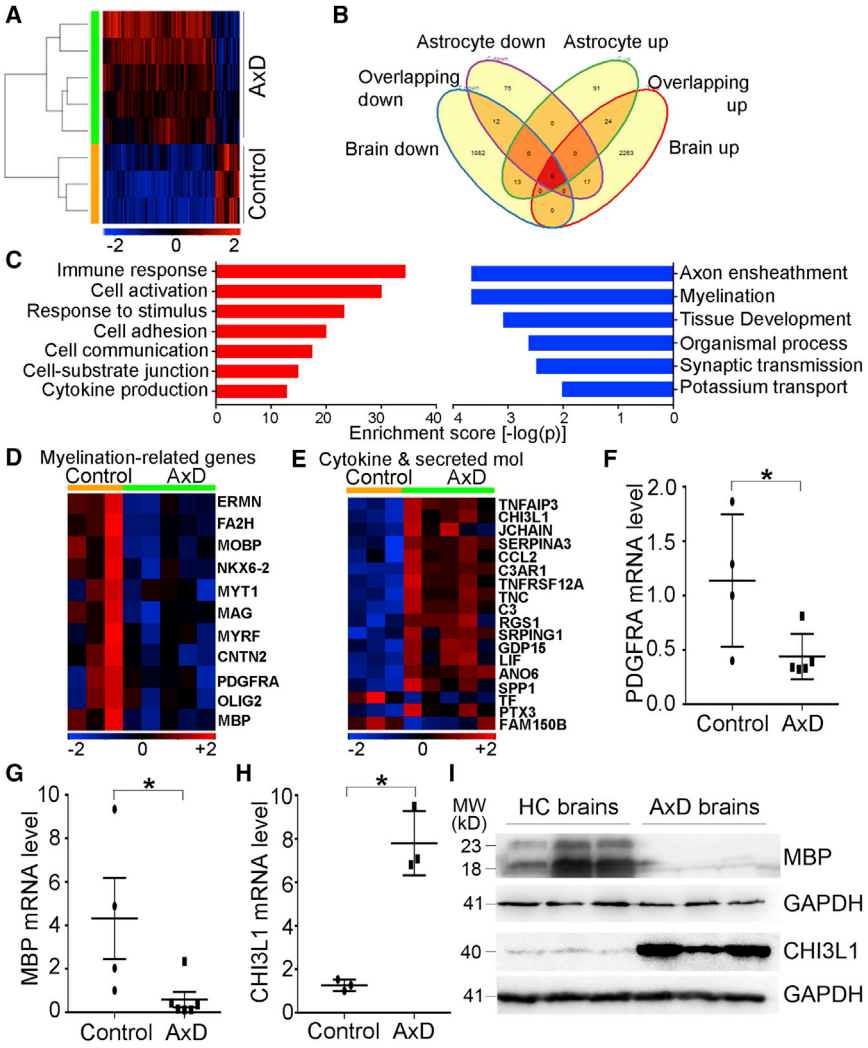

Figure 5. Confirmation of *CHI3L1* Gene Expression Change in AxD Patient Brains

(A) Heatmap presentation of RNA-seq analysis of postmortem brain tissues from AxD patients (AxD) and non-AxD controls. Genes upregulated in AxD brains are shown in red, while genes downregulated are shown in blue.

(B) Venn diagram presentation of genes that show consistent changes in AxD astrocytes and brain tissues, compared to control samples.

(C) GO terms of genes upregulated (red) and downregulated (blue) in both AxD astrocytes and brain tissues, compared to corresponding controls. x axis is enrichment score. Full names of abbreviated GO terms are axon ensheathment in central nervous system (Axon ensheathment), central nervous system myelination (Myelination), multicellular organismal process (Organismal process), and potassium ion transport (Potassium transport).

(D) Heatmap presentation of myelination-related genes downregulated (blue) in AxD brain tissues compared to control brain tissue.

(E) Heatmap presentation of representative genes encoding cytokines and secreted molecules upregulated (red) or downregulated (blue) in AxD brain tissues compared to control brain tissues.

(F and G) qRT-PCR validation of *PDGFRA* (F) and *MBP* (G) mRNA levels in control and AxD brain tissues.

(H) qRT-PCR validation of *CHI3L1* mRNA levels in control and AxD brain tissues.

Error bars are SD of the mean; n = 3 experimental repeats; *p < 0.05 by Student's t test for (F)–(H).

(I) Western blot of MBP and CHI3L1 in control and AxD brain tissues. GAPDH was included as the loading control.

See also Figures S6 and S7A and Table S4.

In AxD brains, the myelination-related genes, including transcriptional factors that regulate myelin formation (e.g., *ERMN*, *MYRF*, and *NKX5-2*) and components of myelin sheath (e.g., *MOBP*, *MAG*, and *MBP*), were downregulated in the RNA-seq analysis (Figure 5D). The reduced expression of *PDGFRA* and *MBP* in AxD brains was confirmed by qRT-PCR (Figures 5F and 5G). The reduced expression of MBP was further confirmed using western blot (Figure 5I). In addition, representative genes in brain tissues related with cytokine and secreted molecules, and cell membrane components and receptors, are shown (Figures 5E and S6C). Among the top differentially expressed genes, *CHI3L1* was significantly upregulated in AxD brain tissues, which was confirmed by both qRT-PCR and western blot (Figures 5H and 5I), consistent with our observation of upregulated *CHI3L1* expression in AxD astrocytes (Figures 4C and 4D). Moreover, correction of the *GFAP* mutation led to reduced *CHI3L1* expression in AxD999-CR astrocytes, compared to that in AxD999 astrocytes (Figure S7A). This result indicates that the *GFAP* mutation in AxD astrocytes is necessary for the elevated expression of *CHI3L1*.

CHI3L1 Mediates the Inhibitory Effect of AxD Astrocytes on OPC Proliferation and Myelination

Because CHI3L1 is a secreted molecule that is expressed by astrocytes (Bonneh-Barkay et al., 2010b; Singh et al., 2011), we tested whether the conditioned medium (CM) from AxD astrocytes could inhibit OPC proliferation and whether blocking CHI3L1 in AxD CM using a neutralizing antibody could reverse the phenotype. We observed a mild decrease in OPC proliferation upon treatment with AxD999 CM conditioned for 24 hr, as revealed by BrdU and OLIG2 double staining. Significantly reduced OPC proliferation was observed when we treated the co-culture with AxD999 CM conditioned for 48 hr, compared to the treatment with control medium without conditioning (Figures 6A and 6B). Blocking CHI3L1 by a CHI3L1 neutralizing antibody reversed the inhibitory effect on OPC proliferation (Figures 6A and 6B), whereas a control IgG failed to reverse the inhibitory effect (Figure S7B). These results indicate that secreted molecules from AxD astrocytes play an important role in inhibiting OPC proliferation and that CHI3L1 is an important mediator of such an effect.

To further validate the role of astrocytic CHI3L1 in regulating OPC proliferation and myelination, we transfected AxD astrocytes

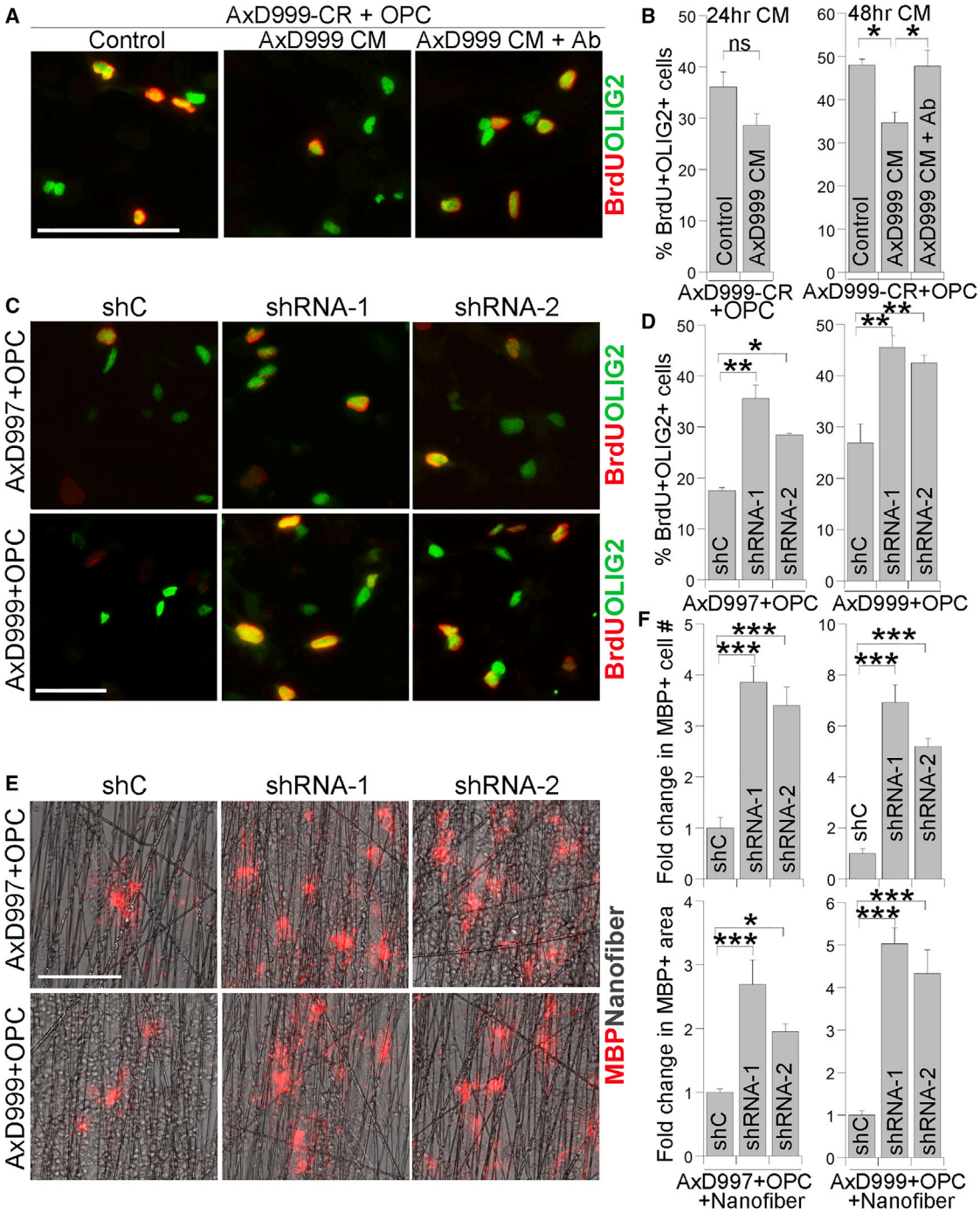

Figure 6. CHI3L1 Mediates the Inhibitory Effect of AxD Astrocytes on OPC Proliferation and Myelination

(A) Representative images of OLIG2 and BrdU staining of AxD999-CR astrocyte-OPC co-cultures treated with control medium, medium conditioned from AxD999 astrocytes for 48 hr (AxD999 CM), or AxD999 CM plus a CHI3L1 neutralizing antibody (Ab).

(B) The percentage of $BrdU^+OLIG2^+$ cells in AxD999-CR astrocyte-OPC co-cultures treated with control medium, medium conditioned from AxD999 astrocytes for 24 or 48 hr, or medium conditioned from AxD999 astrocytes for 48 hr plus a CHI3L1 neutralizing antibody (Ab).

(C and D) Representative images of OLIG2 and BrdU staining and the percentage of $BrdU^+OLIG2^+$ cells in OPCs co-cultured with AxD astrocytes treated with control shRNA (shC) or *CHI3L1*-targeting shRNAs (shRNA-1 and shRNA-2).

(E and F) Representative images of MBP staining and fold change of MBP^+ cell number or MBP^+ area in 3D nanofiber cultures with OPCs and AxD astrocytes treated with shC or *CHI3L1*-targeting shRNAs (shRNA-1 and shRNA-2).

Error bars are SD of the mean; *p < 0.05, **p < 0.01, ***p < 0.001 by one-way ANOVA. See also Figure S7.

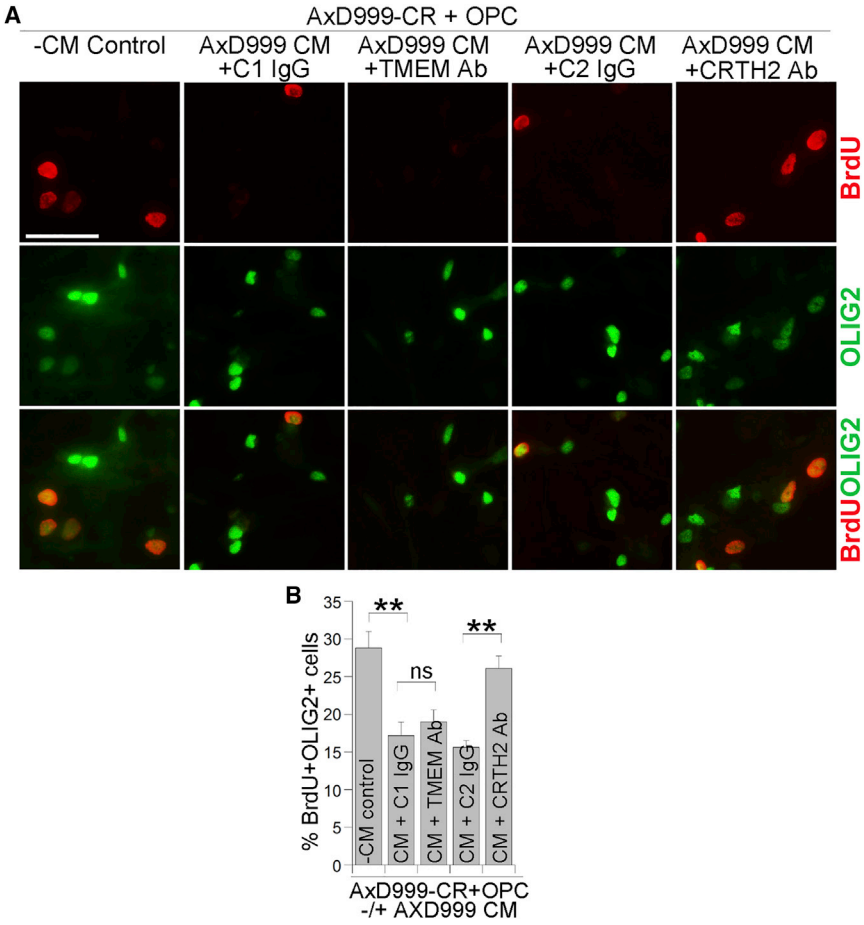

Figure 7. A Neutralizing Antibody for CRTH2 Rescues the AxD999 Astrocyte CM-Induced Reduction of OPC Proliferation

(A) Representative images of OLIG2 and BrdU staining of AxD999-CR astrocyte-OPC co-culture treated with control medium (−CM Control), medium conditioned from AxD999 astrocytes for 48 hr (AxD999 CM) together with a control IgG, or a neutralizing antibody (Ab) for TMEM219 or CRTH2. Sheep IgG (C1 IgG) was included as a negative control for sheep anti-TMEM219 and rabbit IgG (C2 IgG) as a negative control for rabbit anti-CRTH2.

(B) The percentage of $BrdU^+OLIG2^+$ cells in OPCs co-cultured with AxD999-CR astrocytes and treated with control medium, AxD999 CM together with a control IgG, or a neutralizing Ab for TMEM219 or CRTH2.

Error bars are SD of the mean; n = 3 experimental repeats; $^{**}p < 0.01$ by one-way ANOVA. ns, non-significant. See also Figure S7.

with two short hairpin RNAs (shRNAs) (shRNA-1 and shRNA-2) targeting different regions of the *CHI3L1* gene or a control shRNA (shC). The knockdown (KD) of *CHI3L1* mRNA level in the *CHI3L1* shRNA-treated astrocytes was confirmed using qRT-PCR (Figure S7C). KD of *CHI3L1* in AxD astrocytes increased the number of $OLIG2^+$ cells (Figures S7D and S7E) and enhanced the proliferation of OPCs co-cultured with these astrocytes, compared to that in co-culture with shC-treated AxD astrocytes (Figures 6C and 6D). Using the 3D nanofiber-based OPC-astrocyte co-culture system, we found that KD of *CHI3L1* in AxD astrocytes increased the number of MBP^+ cells and the area of MBP-covered nanofibers (MBP^+ area) in OPC co-culture with AxD astrocytes (Figures 6E and 6F). This result demonstrates that KD of *CHI3L1* in AxD astrocytes could ameliorate the inhibitory effect of AxD astrocytes on OPC proliferation and myelination. These results together suggest that CHI3L1 could play an important role in negatively regulating OPC proliferation and myelination.

The effect of CHI3L1 has been shown to be mediated by its receptor IL-13Rα2 and coreceptor TMEM219, or by the receptor CRTH2 (He et al., 2013; Zhou et al., 2014, 2015; Lee et al., 2016). To explore potential receptors for CHI3L1 on OPCs, we checked the expression of the putative CHI3L1 binding partners on OPCs by live staining. While robust expression of IL-13Rα2 was detected on human fibrosarcoma HT1080 cells, no expression of IL-13Rα2 was detected on OPCs (Figure S7F). Expression of CRTH2 and TMEM219 was observed on OPCs, but not astrocytes (Figure S7F). To determine if CHI3L1 could act through CRTH2 or TMEM219 to regulate OPC proliferation, we blocked CRTH2 or TMEM219 in the AxD999-CR astrocyte-OPC co-culture using their respective antibodies. Treatment of the co-culture with the CM of AxD999 astrocytes together with the CRTH2 antibody led to substantial rescue of the AxD999 astrocyte CM-induced reduction of OPC proliferation, whereas treatment with the AxD999 CM together with the TMEM219 antibody had minimal effect (Figures 7A and 7B). This result suggests that the astrocytic CHI3L1 could regulate OPC proliferation by binding to the OPC surface receptor CRTH2. To examine whether there is a species difference in CRTH2 expression in OPCs between mouse and human, we compared the expression level of *CRTH2* in mouse and human OPCs. Reduced level of *CRTH2* mRNA expression was detected in mouse OPCs, compared to human OPCs (Figure S7G). This result indicates that there is a species difference in *CRTH2* expression in OPCs, which may partly contribute to the species difference of dysmyelination phenotype between mouse and human.

DISCUSSION

In this study, we developed a human cellular model for AxD using patient iPSC-derived glial cells. Although transgenic mouse models have been created for AxD (Messing et al., 1998; Hagemann et al., 2005, 2006; Tanaka et al., 2007a), none have yet captured all the key phenotypes of the disease, including abnormalities of myelination and white matter, important pathological phenotypes in AxD patients, especially the early-onset patients (Messing et al., 2001; van der Knaap et al., 2001). In this study, we generated hiPSCs from AxD patients and established a co-culture system using hiPSC-derived astrocytes and OPCs to study the effect of astrocytes on oligodendroglial lineage cells and myelination. This co-culture system allowed us to

recapitulate reduced myelination induced by AxD astrocytes and provided a platform for us to identify molecular and cellular mechanisms underlying myelination defect in AxD.

By comparing the transcriptome of astrocytes derived from AxD and HC iPSCs, we identified a set of differentially expressed genes. GO analysis revealed that genes involved in cytokine activation and cell membrane are among the upregulated GO terms. Upregulation of genes involved in cytokine production and inflammatory response has also been observed in AxD mouse models and patient brain tissues (Olabarria et al., 2015), supporting the validity of our cellular model. During the course of this manuscript preparation, a paper on AxD iPSC-derived astrocytes was published, showing that AxD astrocytes secrete more interleukin cytokines, including IL5, IL6, and TNFα (Kondo et al., 2016), further supporting the involvement of inflammatory response in AxD. Whether the altered expression of these cytokines results from *GFAP* mutations and whether it can be detected in AxD patient brains remain to be tested.

In this study, we identified *CHI3L1* as a gene that is substantially upregulated in AxD iPSC-derived astrocytes, compared to control astrocytes. CHI3L1 is a secreted protein from astrocytes, increased expression of which has been linked to neuroinflammatory conditions (Bonneh-Barkay et al., 2012). It has been used as a biomarker for a variety of inflammation-associated diseases (Bhardwaj et al., 2015), including Alzheimer's disease (Craig-Schapiro et al., 2010; Gispert et al., 2016), amyotrophic lateral sclerosis (Sanfilippo et al., 2017), multiple sclerosis (Bonneh-Barkay et al., 2010a; Hinsinger et al., 2015; Burman et al., 2016), and schizophrenia (Arion et al., 2007). Using isogenic astrocytes, we demonstrated that the *GFAP* mutation in AxD astrocytes is critical for the increased *CHI3L1* expression. Correction of the *GFAP* mutation reversed the elevated expression of *CHI3L1* in AxD astrocytes. We further confirmed the elevated expression of *CHI3L1* in brain tissues from multiple AxD patients and established a causative link between astrocytic *CHI3L1* expression and OPC proliferation/myelination. Moreover, our study using a neutralizing antibody against CRTH2 suggests that the astrocytic CH13L1 could act by binding to the OPC surface receptor CRTH2 to suppress OPC proliferation. CRTH2 has been shown to be involved in cell-cell interactions during inflammatory responses (Harizi, 2013; Taketomi et al., 2013). The CHI3L1/CRTH2 signaling could inhibit OPC proliferation through modulation of intracellular signaling that is important for cell proliferation. The regulation of OPC proliferation could in turn impact myelination. Of note, because the myelination defect, an important patient phenotype, could not be recapitulated in AxD animal models, our observation using the *in vitro* myelination system remains to be validated in an *in vivo* setting.

In summary, in this study, we have developed an hiPSC-based cellular model for a fatal neurological disease, AxD. Our data uncovered a mechanism underlying the myelination defect, a major pathological phenotype of AxD patients that could not be recapitulated in current animal models. In addition to serving as a platform to study AxD mechanisms, this system could also be used to test the effect of potential therapeutic tools and screen drugs for AxD and related leukodystrophy disorders. Indeed, using this human cellular platform, we showed that a neutralizing antibody against CHI3L1 or CRTH2 was able to reverse the inhibitory effect of AxD astrocytes on OPC proliferation. Likewise, *CHI3L1* shRNAs were able to rescue the defective OPC proliferation and reduce myelination induced by AxD astrocytes. These results demonstrate the potential of the iPSC-based AxD cellular model for future AxD drug discovery and validation. Therefore, the study of dysfunction in astrocytes derived from AxD iPSCs is of great importance not only for understanding the pathological mechanisms of AxD, but also for drug discovery to enable better treatment of this so far incurable disease.

Astrocyte dysfunction is involved in the pathogenesis of a wide variety of neurological diseases, including Alzheimer's, Parkinson's, and Huntington's disease; multiple sclerosis; and amyotrophic lateral sclerosis (Rempe and Nedergaard, 2010). However, the specific effects of astrocyte dysfunction on neurodegeneration cannot be easily dissected by studying these diseases because they are complex conditions that also involve dysfunctions of other cell types, including neurons, oligodendrocytes, and immune cells (Messing et al., 2012). AxD is unique among the neurodegenerative diseases because its primary pathological cause is astrocyte dysfunction. Therefore, the study of AxD offers the rare opportunity to identify astrocyte functions that are required for brain development and involved in pathological brain conditions, and to identify treatments that can restore astrocyte functions. It is expected that the knowledge gained through this study could be applicable to the study and treatment of many more common neurological diseases that also have astrocyte abnormalities.

STAR★METHODS

Detailed methods are provided in the online version of this paper and include the following:

- KEY RESOURCES TABLE
- CONTACT FOR REAGENT AND RESOURCE SHARING
- EXPERIMENTAL MODEL AND SUBJECT DETAILS
  - Derivation of iPSCs from Fibroblasts of AxD Patients and Healthy Controls
  - Primary cell cultures
  - Animals
- METHOD DETAILS
  - Generation of Isogenic iPSCs Using CRISPR/Cas9 Nickase
  - Differentiation of Astrocytes from Human iPSCs
  - Differentiation of OPCs and Oligodendrocytes from Human iPSCs
  - Immunohistochemistry
  - Lentiviral Preparation and Transduction
  - Cell Sorting
  - Calcium Imaging
  - Electrophysiology
  - Astrocyte Transplantation
  - Astrocyte-OPC Co-culture
  - 3D Nanofiber Myelination Assay
  - RNA-seq
  - Human Post-mortem Tissue Processing
  - qRT-PCR
  - Western Blot
  - Conditioned Medium Preparation and Neutralizing Antibody Treatment

SUPPLEMENTAL INFORMATION

Supplemental Information includes seven figures and seven tables and can be found with this article online at https://doi.org/10.1016/j.stem.2018.07.009.

ACKNOWLEDGMENTS

We thank Drs. Fred Gage and Alysson Muotri for providing the pBOB-hGFAP::GFP and pBOB-hGFAP::tdTomato plasmids for validation of the pHIV-hGFAP-GFP reporter. We thank Dr. Stephen Forman for sharing the HT1080 cells and IL-13Rα2 antibody as controls. We thank Dr. Feng Zhang for his guidance on CRISPR/Cas9 gene editing. We thank Dr. Albee Messing for his help with interpreting the Rosenthal fiber data and guidance about AxD. We thank Dr. Su-Chun Zhang for his advice on differentiation of hiPSCs into astrocytes. We thank Dr. Xueli Liu for her advice on statistical analysis. We thank Dr. John Zaia for his advice on grammar. We thank Dr. Lu Yang for her help with RNA-seq data submission to GEO. We thank NIH Neurobiobank for providing human postmortem brain tissues. This work was supported by the Herbert Horvitz Family, Sidell Kagan Foundation, California Institute for Regenerative Medicine RB4-06277 and TRAN1-08525, and the National Institute on Aging of the NIH R01AG056305 (Y.S.), the Kimmel Foundation, the Melanoma Research Alliance, and the National Human Genome Research Institute of the NIH R00-HG008171 and DP2-HG010099 (N.E.S.). Guoqiang Sun and J.C. were Herbert Horvitz Fellows. Research reported in this publication was also supported by the National Cancer Institute of the NIH under the award number P30CA33572, and included work performed in the Integrative Genomics, DNA/RNA, Light Microscopy, Electron Microscopy, Pathology, and Analytical Cytometry Cores supported by the National Cancer Institute of the NIH under award number P30CA33572. The content is solely the responsibility of the authors and does not necessarily represent the official views of the NIH.

AUTHOR CONTRIBUTIONS

Y.S. conceived the project. Y.S. and L.L. designed experiments and interpreted results. L.L. performed experiments. L.L. and E.T. generated isogenic iPSCs. E.T. performed qPCR experiments for RNA-seq gene validation and immunostaining analysis, and prepared GFAP-GFP lentivirus. L.L., X.C., and J.C. generated astrocytes. Q.Q. and L.L. generated iPSCs. J.K. performed STR assay, teratoma formation assay, and astrocyte transplantation. Guihua Sun performed DNA methylation analysis, prepared the pHIV-GFAP-GFP reporter construct, and designed the *CHI3L1* shRNA constructs. Guoqiang Sun performed and analyzed Ca^{2+} imaging. Y.H. performed whole-cell patch-clamp recording and astrocyte transplantation. P.Y. harvested and sectioned brain tissues from transplanted mice. X.L. packaged the GFAP-GFP lentivirus. C.D.W. performed raw reads analysis using DESeq2 and goseq and L.L. generated customized gene lists and bar plots for RNA-seq analysis. L.F. prepared OPCs for KD assay. Q.C. designed primers for qRT-PCR analysis. L.L. and A.S. performed CRISPR off-target mutation analysis. P.D. and V.F. provided technical support for OPC differentiation. A.D.R. supported DNA methylation analysis and viral vector preparation. N.E.S. provided technical support for CRISPR/Cas9 gene editing. L.L. and Y.S. prepared the manuscript with input from other authors.

DECLARATION OF INTERESTS

N.E.S. is listed as an inventor on patent applications for genome engineering.

Received: December 18, 2017
Revised: April 23, 2018
Accepted: July 16, 2018
Published: August 2, 2018

REFERENCES

Abbott, N.J., Rönnbäck, L., and Hansson, E. (2006). Astrocyte-endothelial interactions at the blood-brain barrier. Nat. Rev. Neurosci. *7*, 41–53.

Allen, N.J., and Eroglu, C. (2017). Cell biology of astrocyte-synapse interactions. Neuron *96*, 697–708.

Anders, S., Pyl, P.T., and Huber, W. (2015). HTSeq–a Python framework to work with high-throughput sequencing data. Bioinformatics *31*, 166–169.

Arion, D., Unger, T., Lewis, D.A., Levitt, P., and Mirnics, K. (2007). Molecular evidence for increased expression of genes related to immune and chaperone function in the prefrontal cortex in schizophrenia. Biol. Psychiatry *62*, 711–721.

Ashburner, M., Ball, C.A., Blake, J.A., Botstein, D., Butler, H., Cherry, J.M., Davis, A.P., Dolinski, K., Dwight, S.S., Eppig, J.T., et al.; The Gene Ontology Consortium (2000). Gene ontology: tool for the unification of biology. Nat. Genet. *25*, 25–29.

Benjamini, Y., and Hochberg, Y. (1995). Controlling the false discovery rate: a practical and powerful approach to multiple testing. J. R. Stat. Soc. B *57*, 289–300.

Bhardwaj, R., Yester, J.W., Singh, S.K., Biswas, D.D., Surace, M.J., Waters, M.R., Hauser, K.F., Yao, Z., Boyce, B.F., and Kordula, T. (2015). RelB/p50 complexes regulate cytokine-induced YKL-40 expression. J. Immunol. *194*, 2862–2870.

Bonneh-Barkay, D., Wang, G., Starkey, A., Hamilton, R.L., and Wiley, C.A. (2010a). In vivo CHI3L1 (YKL-40) expression in astrocytes in acute and chronic neurological diseases. J. Neuroinflammation *7*, 34.

Bonneh-Barkay, D., Zagadailov, P., Zou, H., Niyonkuru, C., Figley, M., Starkey, A., Wang, G., Bissel, S.J., Wiley, C.A., and Wagner, A.K. (2010b). YKL-40 expression in traumatic brain injury: an initial analysis. J. Neurotrauma *27*, 1215–1223.

Bonneh-Barkay, D., Bissel, S.J., Kofler, J., Starkey, A., Wang, G., and Wiley, C.A. (2012). Astrocyte and macrophage regulation of YKL-40 expression and cellular response in neuroinflammation. Brain Pathol. *22*, 530–546.

Burman, J., Raininko, R., Blennow, K., Zetterberg, H., Axelsson, M., and Malmeström, C. (2016). YKL-40 is a CSF biomarker of intrathecal inflammation in secondary progressive multiple sclerosis. J. Neuroimmunol. *292*, 52–57.

Clarke, L.E., and Barres, B.A. (2013). Emerging roles of astrocytes in neural circuit development. Nat. Rev. Neurosci. *14*, 311–321.

Colombo, E., and Farina, C. (2016). Astrocytes: key regulators of neuroinflammation. Trends Immunol. *37*, 608–620.

Craig-Schapiro, R., Perrin, R.J., Roe, C.M., Xiong, C., Carter, D., Cairns, N.J., Mintun, M.A., Peskind, E.R., Li, G., Galasko, D.R., et al. (2010). YKL-40: a novel prognostic fluid biomarker for preclinical Alzheimer's disease. Biol. Psychiatry *68*, 903–912.

Cui, Q., Yang, S., Ye, P., Tian, E., Sun, G., Zhou, J., Sun, G., Liu, X., Chen, C., Murai, K., et al. (2016). Downregulation of TLX induces TET3 expression and inhibits glioblastoma stem cell self-renewal and tumorigenesis. Nat. Commun. *7*, 10637.

Cui, Q., Shi, H., Ye, P., Li, L., Qu, Q., Sun, G., Sun, G., Lu, Z., Huang, Y., Yang, C.G., et al. (2017). m^6A RNA methylation regulates the self-renewal and tumorigenesis of glioblastoma stem cells. Cell Rep. *18*, 2622–2634.

Domingues, H.S., Portugal, C.C., Socodato, R., and Relvas, J.B. (2016). Oligodendrocyte, astrocyte, and microglia crosstalk in myelin development, damage, and repair. Front. Cell Dev. Biol. *4*, 71.

Douvaras, P., and Fossati, V. (2015). Generation and isolation of oligodendrocyte progenitor cells from human pluripotent stem cells. Nat. Protoc. *10*, 1143–1154.

Ehrlich, M., Mozafari, S., Glatza, M., Starost, L., Velychko, S., Hallmann, A.L., Cui, Q.L., Schambach, A., Kim, K.P., Bachelin, C., et al. (2017). Rapid and efficient generation of oligodendrocytes from human induced pluripotent stem cells using transcription factors. Proc. Natl. Acad. Sci. USA *114*, E2243–E2252.

Gispert, J.D., Monté, G.C., Falcon, C., Tucholka, A., Rojas, S., Sánchez-Valle, R., Antonell, A., Lladó, A., Rami, L., and Molinuevo, J.L. (2016). CSF YKL-40

and pTau181 are related to different cerebral morphometric patterns in early AD. Neurobiol. Aging *38*, 47–55.

Hagemann, T.L., Gaeta, S.A., Smith, M.A., Johnson, D.A., Johnson, J.A., and Messing, A. (2005). Gene expression analysis in mice with elevated glial fibrillary acidic protein and Rosenthal fibers reveals a stress response followed by glial activation and neuronal dysfunction. Hum. Mol. Genet. *14*, 2443–2458.

Hagemann, T.L., Connor, J.X., and Messing, A. (2006). Alexander disease-associated glial fibrillary acidic protein mutations in mice induce Rosenthal fiber formation and a white matter stress response. J. Neurosci. *26*, 11162–11173.

Harizi, H. (2013). The immunobiology of prostanoid receptor signaling in connecting innate and adaptive immunity. BioMed Res. Int. *2013*, 683405.

Hasel, P., Dando, O., Jiwaji, Z., Baxter, P., Todd, A.C., Heron, S., Márkus, N.M., McQueen, J., Hampton, D.W., Torvell, M., et al. (2017). Neurons and neuronal activity control gene expression in astrocytes to regulate their development and metabolism. Nat. Commun. *8*, 15132.

He, C.H., Lee, C.G., Dela Cruz, C.S., Lee, C.M., Zhou, Y., Ahangari, F., Ma, B., Herzog, E.L., Rosenberg, S.A., Li, Y., et al. (2013). Chitinase 3-like 1 regulates cellular and tissue responses via IL-13 receptor α2. Cell Rep. *4*, 830–841.

Hinsinger, G., Galéotti, N., Nabholz, N., Urbach, S., Rigau, V., Demattei, C., Lehmann, S., Camu, W., Labauge, P., Castelnovo, G., et al. (2015). Chitinase 3-like proteins as diagnostic and prognostic biomarkers of multiple sclerosis. Mult. Scler. *21*, 1251–1261.

Hockemeyer, D., and Jaenisch, R. (2016). Induced pluripotent stem cells meet genome editing. Cell Stem Cell *18*, 573–586.

Hrvatin, S., Deng, F., O'Donnell, C.W., Gifford, D.K., and Melton, D.A. (2014). MARIS: method for analyzing RNA following intracellular sorting. PLoS ONE *9*, e89459.

Hsu, F., Kent, W.J., Clawson, H., Kuhn, R.M., Diekhans, M., and Haussler, D. (2006). The UCSC known genes. Bioinformatics *22*, 1036–1046.

Iwaki, T., Kume-Iwaki, A., Liem, R.K., and Goldman, J.E. (1989). Alpha B-crystallin is expressed in non-lenticular tissues and accumulates in Alexander's disease brain. Cell *57*, 71–78.

Johnson, A.B., and Bettica, A. (1989). On-grid immunogold labeling of glial intermediate filaments in epoxy-embedded tissue. Am. J. Anat. *185*, 335–341.

Kim, D., Pertea, G., Trapnell, C., Pimentel, H., Kelley, R., and Salzberg, S.L. (2013). TopHat2: accurate alignment of transcriptomes in the presence of insertions, deletions and gene fusions. Genome Biol. *14*, R36.

Kime, C., Rand, T.A., Ivey, K.N., Srivastava, D., Yamanaka, S., and Tomoda, K. (2015). Practical integration-free episomal methods for generating human induced pluripotent stem cells. Curr. Protoc. Hum. Genet. *87*, 1–21.

Kıray, H., Lindsay, S.L., Hosseinzadeh, S., and Barnett, S.C. (2016). The multifaceted role of astrocytes in regulating myelination. Exp. Neurol. *283* (Pt B), 541–549.

Kondo, T., Funayama, M., Miyake, M., Tsukita, K., Era, T., Osaka, H., Ayaki, T., Takahashi, R., and Inoue, H. (2016). Modeling Alexander disease with patient iPSCs reveals cellular and molecular pathology of astrocytes. Acta Neuropathol. Commun. *4*, 69.

Krencik, R., and Zhang, S.C. (2011). Directed differentiation of functional astroglial subtypes from human pluripotent stem cells. Nat. Protoc. *6*, 1710–1717.

Krencik, R., Weick, J.P., Liu, Y., Zhang, Z.J., and Zhang, S.C. (2011). Specification of transplantable astroglial subtypes from human pluripotent stem cells. Nat. Biotechnol. *29*, 528–534.

Lanciotti, A., Brignone, M.S., Bertini, E., Petrucci, T.C., Aloisi, F., and Ambrosini, E. (2013). Astrocytes: emerging stars in leukodystrophy pathogenesis. Transl. Neurosci. *4*, https://doi.org/10.2478/s13380-013-0118-1.

Lawrence, M., Huber, W., Pagès, H., Aboyoun, P., Carlson, M., Gentleman, R., Morgan, M.T., and Carey, V.J. (2013). Software for computing and annotating genomic ranges. PLoS Comput. Biol. *9*, e1003118.

Lee, S., Leach, M.K., Redmond, S.A., Chong, S.Y., Mellon, S.H., Tuck, S.J., Feng, Z.Q., Corey, J.M., and Chan, J.R. (2012). A culture system to study oligodendrocyte myelination processes using engineered nanofibers. Nat. Methods *9*, 917–922.

Lee, C.M., He, C.H., Nour, A.M., Zhou, Y., Ma, B., Park, J.W., Kim, K.H., Dela Cruz, C., Sharma, L., Nasr, M.L., et al. (2016). IL-13Rα2 uses TMEM219 in chitinase 3-like-1-induced signalling and effector responses. Nat. Commun. *7*, 12752.

Lee, S.H., Nam, T.S., Kim, K.H., Kim, J.H., Yoon, W., Heo, S.H., Kim, M.J., Shin, B.A., Perng, M.D., Choy, H.E., et al. (2017). Aggregation-prone GFAP mutation in Alexander disease validated using a zebrafish model. BMC Neurol. *17*, 175.

Li, L., Chao, J., and Shi, Y. (2018). Modeling neurological diseases using iPSC-derived neural cells : iPSC modeling of neurological diseases. Cell Tissue Res. *371*, 143–151.

Love, M.I., Huber, W., and Anders, S. (2014). Moderated estimation of fold change and dispersion for RNA-seq data with DESeq2. Genome Biol. *15*, 550.

Marchetto, M.C., Brennand, K.J., Boyer, L.F., and Gage, F.H. (2011). Induced pluripotent stem cells (iPSCs) and neurological disease modeling: progress and promises. Hum. Mol. Genet. *20* (R2), R109–R115.

McCarthy, D.J., Chen, Y., and Smyth, G.K. (2012). Differential expression analysis of multifactor RNA-Seq experiments with respect to biological variation. Nucleic Acids Res. *40*, 4288–4297.

Messing, A., Head, M.W., Galles, K., Galbreath, E.J., Goldman, J.E., and Brenner, M. (1998). Fatal encephalopathy with astrocyte inclusions in GFAP transgenic mice. Am. J. Pathol. *152*, 391–398.

Messing, A., Goldman, J.E., Johnson, A.B., and Brenner, M. (2001). Alexander disease: new insights from genetics. J. Neuropathol. Exp. Neurol. *60*, 563–573.

Messing, A., LaPash Daniels, C.M., and Hagemann, T.L. (2010). Strategies for treatment in Alexander disease. Neurotherapeutics *7*, 507–515.

Messing, A., Brenner, M., Feany, M.B., Nedergaard, M., and Goldman, J.E. (2012). Alexander disease. J. Neurosci. *32*, 5017–5023.

Molofsky, A.V., Krencik, R., Ullian, E.M., Tsai, H.H., Deneen, B., Richardson, W.D., Barres, B.A., and Rowitch, D.H. (2012). Astrocytes and disease: a neurodevelopmental perspective. Genes Dev. *26*, 891–907.

Murai, K., Sun, G., Ye, P., Tian, E., Yang, S., Cui, Q., Sun, G., Trinh, D., Sun, O., Hong, T., et al. (2016). The TLX-miR-219 cascade regulates neural stem cell proliferation in neurodevelopment and schizophrenia iPSC model. Nat. Commun. *7*, 10965.

Olabarria, M., Putilina, M., Riemer, E.C., and Goldman, J.E. (2015). Astrocyte pathology in Alexander disease causes a marked inflammatory environment. Acta Neuropathol. *130*, 469–486.

Prust, M., Wang, J., Morizono, H., Messing, A., Brenner, M., Gordon, E., Hartka, T., Sokohl, A., Schiffmann, R., Gordish-Dressman, H., et al. (2011). GFAP mutations, age at onset, and clinical subtypes in Alexander disease. Neurology *77*, 1287–1294.

Qu, Q., Sun, G., Li, W., Yang, S., Ye, P., Zhao, C., Yu, R.T., Gage, F.H., Evans, R.M., and Shi, Y. (2010). Orphan nuclear receptor TLX activates Wnt/beta-catenin signalling to stimulate neural stem cell proliferation and self-renewal. Nat. Cell Biol. *12*, 31–40, 1–9.

Ran, F.A., Hsu, P.D., Lin, C.Y., Gootenberg, J.S., Konermann, S., Trevino, A.E., Scott, D.A., Inoue, A., Matoba, S., Zhang, Y., and Zhang, F. (2013a). Double nicking by RNA-guided CRISPR Cas9 for enhanced genome editing specificity. Cell *154*, 1380–1389.

Ran, F.A., Hsu, P.D., Wright, J., Agarwala, V., Scott, D.A., and Zhang, F. (2013b). Genome engineering using the CRISPR-Cas9 system. Nat. Protoc. *8*, 2281–2308.

Rempe, D.A., and Nedergaard, M. (2010). Targeting glia for treatment of neurological disease. Neurotherapeutics *7*, 335–337.

Sanfilippo, C., Longo, A., Lazzara, F., Cambria, D., Distefano, G., Palumbo, M., Cantarella, A., Malaguarnera, L., and Di Rosa, M. (2017). CHI3L1 and CHI3L2 overexpression in motor cortex and spinal cord of sALS patients. Mol. Cell. Neurosci. *85*, 162–169.

Shi, Y., Chichung Lie, D., Taupin, P., Nakashima, K., Ray, J., Yu, R.T., Gage, F.H., and Evans, R.M. (2004). Expression and function of orphan nuclear receptor TLX in adult neural stem cells. Nature *427*, 78–83.

Shi, Y., Inoue, H., Wu, J.C., and Yamanaka, S. (2017). Induced pluripotent stem cell technology: a decade of progress. Nat. Rev. Drug Discov. *16*, 115–130.

Singh, S.K., Bhardwaj, R., Wilczynska, K.M., Dumur, C.I., and Kordula, T. (2011). A complex of nuclear factor I-X3 and STAT3 regulates astrocyte and glioma migration through the secreted glycoprotein YKL-40. J. Biol. Chem. *286*, 39893–39903.

Sloan, S.A., Darmanis, S., Huber, N., Khan, T.A., Birey, F., Caneda, C., Reimer, R., Quake, S.R., Barres, B.A., and Paşca, S.P. (2017). Human astrocyte maturation captured in 3D cerebral cortical spheroids derived from pluripotent stem cells. Neuron *95*, 779–790.e6.

Sofroniew, M.V., and Vinters, H.V. (2010). Astrocytes: biology and pathology. Acta Neuropathol. *119*, 7–35.

Takahashi, K., Tanabe, K., Ohnuki, M., Narita, M., Ichisaka, T., Tomoda, K., and Yamanaka, S. (2007). Induction of pluripotent stem cells from adult human fibroblasts by defined factors. Cell *131*, 861–872.

Taketomi, Y., Ueno, N., Kojima, T., Sato, H., Murase, R., Yamamoto, K., Tanaka, S., Sakanaka, M., Nakamura, M., Nishito, Y., et al. (2013). Mast cell maturation is driven via a group III phospholipase A2-prostaglandin D2-DP1 receptor paracrine axis. Nat. Immunol. *14*, 554–563.

Tanaka, K., Lee, H.U., and Ikenaka, K. (2007a). [Generation of mice with glial cell dysfunction]. Brain Nerve *59*, 747–753.

Tanaka, K.F., Takebayashi, H., Yamazaki, Y., Ono, K., Naruse, M., Iwasato, T., Itohara, S., Kato, H., and Ikenaka, K. (2007b). Murine model of Alexander disease: analysis of GFAP aggregate formation and its pathological significance. Glia *55*, 617–631.

Tomokane, N., Iwaki, T., Tateishi, J., Iwaki, A., and Goldman, J.E. (1991). Rosenthal fibers share epitopes with alpha B-crystallin, glial fibrillary acidic protein, and ubiquitin, but not with vimentin. Immunoelectron microscopy with colloidal gold. Am. J. Pathol. *138*, 875–885.

van der Knaap, M.S., Naidu, S., Breiter, S.N., Blaser, S., Stroink, H., Springer, S., Begeer, J.C., van Coster, R., Barth, P.G., Thomas, N.H., et al. (2001). Alexander disease: diagnosis with MR imaging. AJNR Am. J. Neuroradiol. *22*, 541–552.

van der Voorn, J.P., Pouwels, P.J., Salomons, G.S., Barkhof, F., and van der Knaap, M.S. (2009). Unraveling pathology in juvenile Alexander disease: serial quantitative MR imaging and spectroscopy of white matter. Neuroradiology *51*, 669–675.

Verkhratsky, A., and Parpura, V. (2016). Astrogliopathology in neurological, neurodevelopmental and psychiatric disorders. Neurobiol. Dis. *85*, 254–261.

Verkhratsky, A., Sofroniew, M.V., Messing, A., deLanerolle, N.C., Rempe, D., Rodríguez, J.J., and Nedergaard, M. (2012). Neurological diseases as primary gliopathies: a reassessment of neurocentrism. ASN Neuro *4*, e00082.

Wang, L., Colodner, K.J., and Feany, M.B. (2011). Protein misfolding and oxidative stress promote glial-mediated neurodegeneration in an Alexander disease model. J. Neurosci. *31*, 2868–2877.

Wang, L., Hagemann, T.L., Kalwa, H., Michel, T., Messing, A., and Feany, M.B. (2015). Nitric oxide mediates glial-induced neurodegeneration in Alexander disease. Nat. Commun. *6*, 8966.

Wen, Z., Nguyen, H.N., Guo, Z., Lalli, M.A., Wang, X., Su, Y., Kim, N.S., Yoon, K.J., Shin, J., Zhang, C., et al. (2014). Synaptic dysregulation in a human iPS cell model of mental disorders. Nature *515*, 414–418.

Young, M.D., Wakefield, M.J., Smyth, G.K., and Oshlack, A. (2010). Gene ontology analysis for RNA-seq: accounting for selection bias. Genome Biol. *11*, R14.

Yu, J., Vodyanik, M.A., Smuga-Otto, K., Antosiewicz-Bourget, J., Frane, J.L., Tian, S., Nie, J., Jonsdottir, G.A., Ruotti, V., Stewart, R., et al. (2007). Induced pluripotent stem cell lines derived from human somatic cells. Science *318*, 1917–1920.

Zhang, Y., Sloan, S.A., Clarke, L.E., Caneda, C., Plaza, C.A., Blumenthal, P.D., Vogel, H., Steinberg, G.K., Edwards, M.S., Li, G., et al. (2016). Purification and characterization of progenitor and mature human astrocytes reveals transcriptional and functional differences with mouse. Neuron *89*, 37–53.

Zhou, Y., Peng, H., Sun, H., Peng, X., Tang, C., Gan, Y., Chen, X., Mathur, A., Hu, B., Slade, M.D., et al. (2014). Chitinase 3-like 1 suppresses injury and promotes fibroproliferative responses in Mammalian lung fibrosis. Sci. Transl. Med. *6*, 240ra76.

Zhou, Y., He, C.H., Herzog, E.L., Peng, X., Lee, C.M., Nguyen, T.H., Gulati, M., Gochuico, B.R., Gahl, W.A., Slade, M.L., et al. (2015). Chitinase 3-like-1 and its receptors in Hermansky-Pudlak syndrome-associated lung disease. J. Clin. Invest. *125*, 3178–3192.

STAR★METHODS

KEY RESOURCES TABLE

REAGENT or RESOURCE	SOURCE	IDENTIFIER
Antibodies		
Rabbit monoclonal anti-NANOG	Cell Signaling	Cat# 4903; RRID: AB_10559205
Mouse monoclonal anti-OCT4	Santa Cruz	Cat# sc-5279; RRID: AB_628051
Goat polyclonal anti-SOX2	Santa Cruz	Cat# sc-17320; RRID: AB_2286684
Mouse monoclonal anti-SSEA4	Santa Cruz	Cat# sc-21704; RRID: AB_628289
Mouse monoclonal IgM anti-Tra-1-60	Santa Cruz	Cat# sc-21705; RRID: AB_628385
Mouse monoclonal IgM anti-Tra-1-81	Santa Cruz	Cat# sc-21706; RRID: AB_628386
Rabbit polyclonal anti-GFAP	DAKO	Cat# N1506; RRID: AB_10013482
Mouse monoclonal anti-GFAP	Sigma-Aldrich	Cat# G3893; RRID: AB_477010
Mouse monoclonal anti-human GFAP	Cellartis	Cat# 40420
Rabbit monoclonal anti-S100 β	Abcam	ab52642; RRID: AB_882426
Mouse polyclonal anti-CRYAB	Enzo Life Sciences	Cat# ADI-SPA-223; RRID: AB_10615646
Goat polyclonal anti-SOX9	R&D Systems	Cat# AF3075; RRID: AB_2194160
Mouse monoclonal anti-NKX2.2	DSHB	Cat# 74.5A5; RRID: AB_531794
Rabbit polyclonal anti-OLIG2	EMD Millipore	Cat# AB9610; RRID: AB_570666
Goat polyclonal anti-OLIG2	R&D Systems	Cat# AF2418; RRID: AB_2157554
Mouse monoclonal IgM anti-O4	Sigma-Aldrich	Cat# O7139; RRID: AB_477662
Rat monoclonal anti-MBP	Millipore	Cat# MAB386; RRID: AB_94975
Rat monoclonal anti-BrdU	Accu-Specs	Cat# OBT-0030; RRID: AB_2341179
Rabbit polyclonal anti-cleaved Caspase-3	Cell Signaling	Cat# 9661; RRID: AB_2341188
Rat monoclonal anti-CD31-PE	BD Biosciences	Cat# 553373; RRID: AB_394819
Rabbit polyclonal anti-FSP1	EMD Millipore	Cat# ABF32; RRID: AB_11203822
Chicken polyclonal anti-MAP2	Abcam	Cat# ab5392; RRID: AB_2138153
Rabbit polyclonal anti-CHI3L1	Abcam	Cat# ab180569
Goat polyclonal anti-CHI3L1	R&D Systems	Cat# AF2599; RRID: AB_2291883
Sheep polyclonal anti-TMEM219	R&D Systems	Cat# AF7556
Rabbit polyclonal anti-CRTH2	Invitrogen	Cat# PA5-34502; RRID: AB_2551854
Bacterial and Virus Strains		
hGFAP-GFP	This paper	N/A
Biological Samples		
Postmortem human brain frontal cortex	NIH NeuroBiobank	RRID: SCR_003131
Chemicals, Peptides, and Recombinant Proteins		
Matrigel	Corning	Cat# CB40230
mTeSR1	Stem Cell Technologies	Cat# 85850
Rocki Y-27632	Reprocell	Cat# 04-0012-10
Accutase	Sigma-Aldrich	Cat# A6964
SB431542	Stemgent	Cat# 04-0010
LDN-193189	Stemgent	Cat#04-0074
Smoothened agonist (SAG)	EMD Millipore	Cat#566660
bFGF	PeproTech	Cat# 100-18B
EGF	PeproTech	Cat#100-15
Retinoic acid	Sigma-Aldrich	Cat#R2625
N2	Life Technologies	Cat# 17502048
B27	Life Technologies	Cat# 12587010
CNTF	R&D systems	Cat# 257-NT-050

(*Continued on next page*)

Continued

REAGENT or RESOURCE	SOURCE	IDENTIFIER
PDGFAA	R&D systems	Cat# 221-AA-050
IGF-1	R&D systems	Cat#291-G1-200
HGF	R&D systems	Cat#294-HG-025
NT3	EMD Millipore	Cat# GF031
3,3′,5-Triiodo-L-thyronine (T3)	Sigma-Aldrich	Cat# T2877
Biotin	Sigma-Aldrich	Cat#4639
cAMP	Sigma-Aldrich	Cat# D0260
L-Ascorbic acid	Sigma-Aldrich	Cat# A4403
Inuslin	Sigma-Aldrich	Cat#I9278
BrdU	Sigma-Aldrich	Cat#B5002
Fluo-4-AM	Invitrogen	Cat# F14201
Critical Commercial Assays		
Tetro cDNA Synthesis kit	BioLINE	Cat#Bio-65043
SYBR Green Master Mix	Thermo Scientific	Cat#F416L
P3 4D nucleofection kit	Lonza	Cat# V4XP-3024
Deposited Data		
RNA-seq data	This paper	GEO: GSE116327
Experimental Models: Cell Lines		
I90 fibroblast	Coriell	Cat#IMR90; RRID: CVCL_0347
C1 fibroblast	ATCC	Cat# CRL-2097; RRID: CVCL_2337
C3 fibroblast	Wen et al., 2014	N/A
AxD825 fibroblast	Coriell	Cat# GM16825; RRID: CVCL_U890
AxD997 fibroblast	Telethon network	Cat# FFF0211997
AxD999 fibroblast	Telethon network	Cat# FFF0211999
Human primary astrocytes	ScienCell	Cat # 1800
Experimental Models: Organisms/Strains		
NSG mice	The Jackson Laboratory	Cat#005557; RRID: IMSR_JAX:005557
Rag2−/− mice	The Jackson Laboratory	Cat#008449; RRID: IMSR_JAX:008449
Oligonucleotides		
See Table S5 for details	N/A	N/A
Recombinant DNA		
pSpCas9n (BB)-2A-GFP	Ran et al., 2013b	#48140
pCXLE-hSK	Addgene	#27078
pCXLE-hUL	Addgene	#27080
pCXLE-hOCT3/4-shp53-F	Addgene	#27077
pCXWB-EBNA1	Addgene	#37624
Software and Algorithms		
Zen 2.3	Carl Zeiss	N/A
Image Pro Premier 9.3	Media Cybernetics	N/A
GraphPad Prism 7.01	GraphPad Software	RRID: SCR_002798

CONTACT FOR REAGENT AND RESOURCE SHARING

Further information and requests for resources and reagents should be directed to and will be fulfilled by the Lead Contact, Yanhong Shi (yshi@coh.org).

EXPERIMENTAL MODEL AND SUBJECT DETAILS

Derivation of iPSCs from Fibroblasts of AxD Patients and Healthy Controls

AxD997 (female) and AxD999 (male) fibroblasts were obtained from Telethon Network, AxD825 (male) fibroblast and control fibroblast I90 (IMR90; female) from Coriell, control fibroblast C1 (CRL-2097; male) from ATCC. All fibroblast lines were reprogrammed using episomal plasmids expressing OCT4, SOX2, L-MYC, KLF4, shp53, and EBNA1 (Addgene plasmids pCXLE-hSK, pCXLE-hUL, pCXLE-hOCT3/4-shp53-F, and pCXWB-EBNA1). Cells electroporated with reprogramming plasmids using 4D Nucleofector (Lonza) were seeded into 6-well plates coated with 1:100 diluted Matrigel (Corning) and maintained in mTeSR1 medium (Stem Cell Technologies). C3 iPSCs were generated and characterized previously (Wen et al., 2014; Murai et al., 2016). iPSCs generated from AxD and control fibroblasts were maintained at 37°C in mTeSR1 medium in Matrigel-coated 6-well plates and passaged every 3-4 days using 0.5 mM EDTA (GIBCO) treatment and manual dissociation. Small clusters of iPSCs were transferred to new plates coated with Matrigel at 1:6 to 1:10 ratio. Medium was changed daily. All iPSC lines generated in this study were authenticated using STR assay.

Primary cell cultures

The human primary astrocytes were purchased from ScienCell Research Laboratories (ScienCell, Cat # 1800) and cultured at 37°C in astrocyte medium (ScienCell, Cat# 1801) containing 500 mL of basal medium, 10 mL of fetal bovine serum, 5 mL of astrocyte growth supplement and 5 mL of penicillin/streptomycin. Gender information of this product is not released by the vendor.

Animals

$Rag2^{-/-}$ mice (The Jackson Laboratory, RRID: IMSR_JAX:008449) were used for astrocyte transplantation and mouse primary OPC isolation. NSG mice (The Jackson Laboratory, RRID: IMSR_JAX:005557) were used for teratoma formation assay. All animal work was performed without gender bias under the Institutional Animal Care and Use Committee (IACUC) protocol approved by the City of Hope IACUC Committee.

METHOD DETAILS

Generation of Isogenic iPSCs Using CRISPR/Cas9 Nickase

The pSpCas9n (BB)-2A-GFP plasmid containing Cas9n (D10A nickase mutant) with 2A-EGFP and cloning backbone for sgRNA was purchased from Addgene (Plasmid #48140). Guide RNAs were designed to generate DNA double-strand breaks that cover M73K mutation site using an online designing tool (http://crispr.mit.edu/). The oligonucleotides for sgRNA were synthesized by Integrated DNA Technologies (IDT) and cloned to pSpCas9n (BB)-2A-GFP plasmid according to previously published protocol (Ran et al., 2013b). The single-strand donor DNA (ssODN) contains A to T correction at the M73K mutation site of the human *GFAP* gene, and includes a silent G to A mutation at one of the protospacer adjacent motif (PAM) sites to avoid repeated cutting by Cas9n. Another silent mutation, C to G, was introduced to create AgeI digestion site that allowed identification of clones with successful homologous recombination. The sequences of sgRNAs and ssODNs were summarized in Table S4. AxD999 iPSCs were transfected with the CRISPR/Cas9n plasmid and the ssODN using 4D Nucleofector (Lonza). After electroporation, cells were seeded onto Matrigel-coated plates and cultured in mTeSR1 medium supplemented with 10 μM Rock Inhibitor for overnight. The next day, cells were fed with fresh mTeSR1 medium. Cells were harvested 2 days after electroporation and sorted using GFP-based FACS. The sorted cells were plated at low density and maintained in mTeSR1 medium for about 10 to 14 days to allow colony formation from single cells.

To screen for gene-corrected clones, individual colonies were manually split to 2 halves. One half was used for genomic DNA (gDNA) extraction and the other half was seeded into 48-well plates for maintenance. PCR was performed to amplify regions covering the M73K mutation site using genomic DNA as the template. The PCR products were digested using AgeI restriction enzyme. Clones that could be digested by AgeI were further analyzed by Sanger sequencing to confirm the correction of M73K mutation site. The potential off-target sites were predicted by an online tool (https://www.sanger.ac.uk/htgt/wge/find_off_targets_by_seq). The off-target sites containing 0-3 mismatches with sgRNAs were PCR-amplified and sequenced by Sanger sequencing. The off-target site sequences, PCR primers and analysis results are listed in Table S6.

Differentiation of Astrocytes from Human iPSCs

For astrocyte differentiation (Table S7), human iPSCs (I90, C1, AxD825, AxD999, AxD999-CR) were first differentiated into neural progenitor cells (NPCs) by treating with 10 μM SB434542 (Stemgent), 250 nM LDN-193189 (Stemgent) and 10 μM retinoic acid (RA; Sigma-Aldrich) for 8 days. NPCs were further differentiated by treatment of 10 μM RA and smoothened agonist (SAG; EMD Millipore) for 4 days. Then cells were dissociated using Accutase and allowed to form spheres in suspension culture for 8 days, which contains 1X N2 (Life Technologies), 1XB27 (Life Technologies), 10 μM RA and 10 μM SAG. Spheres were attached on Matrigel-coated plates and cultured in PDGF medium containing 1X N2, 1XB27, 10 ng/ml PDGFAA (R&D Systems), 5 ng/ml HGF (R&D Systems), 10 ng/ml IGF-1 (R&D Systems), 10 ng/ml NT3 (EMD Millipore), 100 ng/ml Biotin (Sigma-Aldrich), 60ng/ml T3 (Sigma-Aldrich), 1 μM cAMP (Sigma-Aldrich) and 25 μg/ml insulin (Sigma-Aldrich). After 10 days of culture, astrocytes migrated out of the spheres were dissociated using Accutase into single cells and seeded into astrocyte medium, containing 1X N2, 1X B27, 10 ng/ml EGF (Peprotech) and

10 ng/ml FGF (Peprotech). These astrocytes were passaged twice a week for another 2 weeks. For final maturation of astrocytes, 10 ng/ml CNTF (R&D Biosciences) was supplemented to medium containing 1X N2 and 1X B27 for 1 week. To show that the relevant cellular phenotypes could be recapitulated in iPSC-derived astrocytes independent of the differentiation protocol, a pair of control and AxD iPSCs (C3 and AxD997) were also differentiated into astrocytes following a previously published protocol (Krencik and Zhang, 2011). Briefly, iPSCs were collected for suspension culture to allow embryo body (EB) formation. EBs were induced to neural lineage by medium supplemented with 1X N2 for 1 week. After 1 week, EBs were attached and rosette-like neuroepithelial structures were able to form within another week. Rosettes were manually blown-off and cultured as spheres in N2 medium supplemented with 10 ng/ml EGF and 10 ng/ml FGF. Spheres were dissociated once a week until day 120 of differentiation. Astrocytes beyond day120 of differentiation from both protocols were used for experiments.

Differentiation of OPCs and Oligodendrocytes from Human iPSCs

We followed a previously published protocol (Douvaras and Fossati, 2015) for differentiation of human iPSCs into OPCs and oligodendrocytes. Briefly, human iPSC were singlized and treated with SB434542, LDN-193189 and RA for 8 days. From Day 8 to 12, cells were further induced by RA and smoothened agonist (SAG). After RA and SAG induction, pre-OPCs expressing OLIG2 and NKX2.2 markers were lift up to form spheres. Pre-OPC spheres were cultured in RA and SAG-supplemented medium for another 8 days, then switched to PDGF medium. 10 Days after switching to PDGF medium, spheres were attached onto Matrigel coated-plates to allow OPCs to migrate out of the spheres and expand. Medium was changed every 2 days. $O4^+$ OPCs could be detected by live staining using O4 antibody around 30 days after sphere attachment. MBP^+ mature oligodendrocytes can be generated in another 2 weeks by culturing in maturation medium that has the growth factors, PDGF, IGF, HGF and NT3, withdrawn from the PDGF medium.

Immunohistochemistry

Cells were fixed with 4% paraformaldehyde (PFA) for 15 min, permeabilized with 0.1% Triton X-100 for 1 hr, and blocked with 5% donkey serum for 1 hr at room temperature (RT). Cells were then incubated with primary antibody diluted in PBS containing 0.1% Triton X-100 and 5% donkey serum and incubated for overnight at 4°C. On the following day, cells were incubated with the relevant secondary antibody diluted at 1:500 in PBS for 1 hr at RT. Cells were counterstained with DAPI before mounting.

For BrdU labeling, OPCs were incubated with 10 μM BrdU for 6 hr, while astrocytes were incubated for 4 hours, and then fixed by 4% PFA for BrdU staining. OPCs were stained with the nucleus marker OLIG2 first. After OLIG2 staining, cells were re-fixed using 4% PFA at RT for 15 min. Cells were then treated with 2 N HCL at 37°C for 30 min followed by Borate buffer incubation at RT for 15 min. BrdU was stained using anti-BrdU primary antibody and appropriate secondary antibody. Cells were counterstained with DAPI. Antibodies used in this study are listed in Key Resources Table.

Lentiviral Preparation and Transduction

The pHIV-hGFAP-GFP lentiviral vector was prepared by cloning the hGFAP-GFP fragment from the hGFAP-GFP vector (Addgene, plasmid #40592) into the pHIV vector. Lentiviruses were prepared as previously described (Shi et al., 2004; Qu et al., 2010). To transduce astrocytes, cells were seeded onto Matrigel-coated plates for overnight and then transduced with the pHIV-hGFAP-GFP lentivirus supplemented with 4 μg/ml polybrene (AmericanBio) for 24 hr. Virus-containing medium was replaced with fresh astrocyte culture medium 24 hr later.

Cell Sorting

The pHIV-hGFAP-GFP lentivirus-transduced astrocytes were sorted using ARIA SORP cell sorter (BD Bioscience) at the Analytical Cytometry Core at City of Hope. Astrocytes without viral transduction were used as the negative control. The GFP^+ cells were collected into astrocyte culture medium and propagated for experiments. The $O4^+$ OPCs were sorted using magnetic-activated cell sorting (MACS) following manufacturer's (Miltenyi Biotech) instruction. The OPC differentiation product was dissociated into single cells using Accutase. These cells were incubated with O4-microbeads at 4°C for 15 min, protected from light. Cell suspension was loaded onto LS Magnetic Column (Miltenyi Biotech) placed in the field of a magnetic MACS Separator. The $O4^-$ cells were washed off, while the $O4^+$ OPCs were retained, followed by elution into collection tube. The $O4^+$ OPCs were counted using hemacytometer and used for astrocyte co-culture experiments.

Calcium Imaging

Cells were matured in CNTF medium on Matrigel-coated iBibi 8-well chamber slides for at least 5 days before imaging. 2 μM Fluo-4 AM (Invitrogen) was loaded onto cells for 15 minutes and then washed 3 times with PBS. 0.4 mL culture medium was added per chamber to replace PBS. 3 minutes later, cells were imaged at 0.7 s intervals using 20X objective of Zeiss Observer Z1 microscope with heat and CO_2 controlled live imaging chamber. For the pharmacological experiment, ATP (3 μM) was applied at around 50 s after starting recording. To quantify the percentage of cells responding to ATP stimulation, fluorescence levels were quantified using ImagePro software. The change of fluorescence level over time is defined as $\Delta F/F = (F - F_0)/F_0$, where F is the fluorescence intensity at any time point, and F_0 is the baseline fluorescence intensity averaged across the whole movie for each cell. Cells with $\Delta F/F > 0.05$ were counted as responsive. Intensity traces of cells were extracted using ImagePro Premium 9.3 (Media Cybernetics) and used to calculate and graph the fluctuations of Ca^{2+} intensity.

Electrophysiology

Cells were plated in 3.5 mm dishes coated with Matrigel and were analyzed by whole-cell patch clamp recording. Whole-cell patch clamp recording was performed with a voltage clamp at −70 mV and stepped from −50 mV to +50 mV at 10 mV increments for duration of 500 ms. Cells were bathed in Hank's buffered Saline solution (140 mM NaCl, 3 mM KCl, 2 mM $CaCl_2$, 1 mM $MgCl_2$, 15 mM HEPES and 23 mM glucose, pH of 7.35-7.45). Glass pipettes were back filled with intracellular solution (145 mM KCl, 10 mM NaCl, 1mM EGTA, 1mM $MgCl_2$, 10mM HEPEs, pH of 7.35-7.45). Osmolality for both solutions was 300 ± 10 milliosmole (mOsm).

Astrocyte Transplantation

Human iPSC-derived AxD999 astrocytes purified using GFAP-GFP-based FACS were resuspended in astrocyte medium at 100,000 cells/μl. 200,000 cells were injected at 1 mm from the midline between the Bregma and Lambda and 1 mm deep into the anterior lateral ventricles of P2-P4 $Rag2^{-/-}$ mice. The transplanted mice were perfused with 4% PFA 1 month after transplantation. Brains were harvested, embedded in OCT and sectioned at 30 μm thickness. Brain sections were immunostained for human GFAP (hGFAP) and imaged for both hGFAP signal and GFAP-GFP fluorescence.

Astrocyte-OPC Co-culture

Astrocytes were seeded at the density of $5x10^4$ cells per well in Matrigel-coated 24-well plates and induced for maturation by 10 ng/ml CNTF for 5-7 days. The $O4^+$ OPCs sorted by MACS were plated onto astrocyte cultures at $5x10^3$ cells per well. Co-cultured cells were maintained in PDGF medium. For O4 and OLIG2 quantification assays, OPCs were co-cultured with astrocytes for 5 days. On Day 5 of co-culture, cells were fixed and stained as described in the Immunohistochemistry section. For BrdU labeling assay and apoptosis assay, OPCs were co-cultured with astrocytes for 1 day. On Day 2 of co-culture, cells were stained for cleaved Caspase-3 and OLIG2 or BrdU and OLIG2. Images were taken using Zeiss Observer or Nikon ECLIPSE TE2000-S. A minimum of 5 images per well were taken for cell number quantifications.

3D Nanofiber Myelination Assay

Eight-chamber slides aligned with 700 nm diameter electrospun polycaprolactone (PCL) nanofibers were purchased from Nanofiber Solutions. 1:100 diluted Matrigel was used to coat nanofibers at 37°C for 3 days. Astrocytes were seeded at $5x10^4$ cells per chamber and induced for maturation by 10 ng/ml CNTF for 5 days. Then the $O4^+$ OPCs sorted by MACS were seeded at $8x10^4$ cells per chamber. Cells were cultured in OPC medium for 5 days with medium change daily and switched to maturation medium to allow OPC maturation for 2 weeks with medium change every 2 days. After 2 weeks of maturation, cells were fixed with 4% PFA and stained as described in the Immunohistochemistry section. Images were taken using Zeiss Confocal 700. A minimum of 5 images per well were taken for quantification of MBP^+ cell number and MBP^+ area. MBP^+ area and segment length were analyzed by polygon or line drawing using ImagePro. For high resolution images, OPCs were plated on 2 μM aligned naofibers (MIMETIX, Electrospinning Company) as described above and imaged using Zeiss Confocal 880 with Airyscan. 3D images were generated using Zen Blue edition.

RNA-seq

RNA isolation from fixed, $GFAP^+$ sorted astrocytes was performed following a previously published protocol (Hrvatin et al., 2014). Briefly, we fixed astrocytes and stained with GFAP antibody and appropriate secondary antibody. Then the $GFAP^+$ cells were sorted under sterile conditions and collected for RNA isolation. RNase inhibitor was added into staining and sorting buffers to minimize RNA degradation during the procedure. RNA was isolated from the sorted cells using the RecoverAll Total Nucleic Acid Isolation kit (Ambion). RNA quality control and subsequent library construction and poly (A) RNA-seq were performed by the Integrative Genomics Core at City of Hope. RNA-Seq reads were aligned against the human genome (hg19) using TopHat2 (version 2.0.14; Kim et al., 2013). Read counts were quantified using htseq-count (version 0.6.0) (Anders et al., 2015) with UCSC known gene annotations (TxDb.Hsapiens.UCSC.hg19.knownGene, downloaded 6/8/2016) (Hsu et al., 2006). Aligned reads were counted using GenomicRanges (Lawrence et al., 2013). Genes were filtered to only include transcripts with RPKM values greater than 0.1 (after a rounded log2-transformation) in at least 50% of samples. Genes smaller than 150 bp were removed prior to differential expression analysis. Log_2(RPKM + 0.1) expression values were used for visualization and fold-change calculations. Separate comparisons were performed for the 4 astrocyte lines and the 8 brain samples (AxD versus control). We used a 1-variable model for the tissue comparison and a 2-variable model (adjusting for differentiation method) for astrocyte comparison. To determine genes with varied expression between control and AxD in both astrocytes and brain tissue (n = 12), we used a 2-variable model in DESeq2. P values were calculated using DESeq2 (Love et al., 2014), which were used to calculate the False Discovery Rate (FDR) (Benjamini and Hochberg, 1995). Differentially expressed genes (DEG) were defined as FDR < 0.05 and absolute value of fold change > 1.5. The venn diagram was produced using the Vennerable package (version 3.0) in R. Gene Ontology (GO) (Ashburner et al., 2000) enrichment was performed using goseq (Young et al., 2010). Representative genes of each function type were selected based on their functional relevance through literature search and |fold-change| > 1.5. Heatmaps were generated by the gplots package (version 3.0.1). While the 2-variable n = 4 astrocyte comparison using DESeq2 did not strictly identify *CHI3L1*, it could be identified using both a 1-variable n = 4 astrocyte comparison and an n = 8 brain tissue comparison using edgeR (McCarthy et al., 2012), consistent with *CHI3L1* as the top DEG in n = 12 comparison using DESeq2.

Human Post-mortem Tissue Processing

Fixed and frozen brain tissues from post-mortem AxD patients and healthy control individuals were obtained from NIH Neurobiobank (RRID: SCR_003131). The evaluation from Institutional Review Board determined these coded tissues without identifiers from deceased subjects do not meet the definition of human subject research. RNAs from frozen brain tissues were isolated using Trizol (Ambion) as previously described (Cui et al., 2016, 2017). Quality control of RNAs, library construction and poly(A) RNA-seq were performed by the Integrative Genomics Core at City of Hope. Data analysis was performed as described above.

qRT-PCR

Total RNA was extracted using Trizol (Ambion) as previously described (Cui et al., 2016, 2017). Complementary DNA was reverse transcribed from 1 μg total RNA using Tetro cDNA Synthesis kit (BioLINE). Primer sequences are listed in Table S5. qRT-PCR was performed using SYBR Green Master Mix (Thermo Scientific) on the Step One Plus Real-Time PCR Instrument (Applied Biosystems). *ACTIN* or *GAPDH* was used as the reference gene. Each reaction was run in triplicate. Data was analyzed using ΔΔCt method and normalized to control group in each run.

Western Blot

Cell lysates were extracted using Pierce RIPA buffer (Thermo Scientific). Protein concentration was measured using BCA assay kit (Thermo Scientific). 40 μg proteins for CHI3L1 and 30 μg proteins for MBP were loaded for western blot. Western blot membranes were developed using ECL Select kit (GE Healthcare) and imaged using ChemiDoc Imaging System (Bio-Rad).

Conditioned Medium Preparation and Neutralizing Antibody Treatment

AxD999 astrocytes were seeded at 1 million cells/well in a Matrigel-coated 6-well plate. Cells were conditioned in PDGF medium for 24 or 48 hours. Conditioned medium was collected and centrifuged at 200xg for 10 minutes and supernatant was filtered through 0.22 μm filter to eliminate cells and cell debris. The $O4^+$ OPCs were sorted using MACS and eluted with AxD999 conditioned medium. 5,000 OPCs were seeded onto AxD999-CR astrocytes and cultured in AxD999 conditioned medium supplemented with 10 μg/ml neutralizing antibody or corresponding control IgG for 24 hr.

shRNA Preparation and *CHI3L1* Knockdown

shRNAs were cloned into the lentiviral PGK-puro vector. The following shRNA sequences were used: control shRNA, 5′-TCTACTGTC ACTCAGTACC-3′; *CHI3L1* shRNA-1, 5′-ATGCAGAGCAGCACTGGAGC-3′; *CHI3L1* shRNA-2, 5′-ATGGCGGTACTGACTTGATG-3′. 5 μg shRNAs were transfected into astrocytes using Lipofectmin 3000 following manufacturer's instruction (Life Technologies) for co-culture assays that were less than 5 days. For myelination assay that needs co-culture for more than 5 days, shRNA lentiviruses were used to infect astrocytes at MOI of 1.

Mouse OPC Isolation

Neonatal $Rag2^{-/-}$ mice were euthanized and brain tissues were harvested immediately. Brains were dissociated into single cells using Neural Tissue Dissociation Kit (P) (Miltenyi Biotech) and gentleMACS Octo Dissociator with Heaters (Miltenyi Biotech) following manufacturer's instructions. Singlized cells were incubated with O4 antibody-conjugated microbeads and sorted with MACS as described above. $O4^+$ OPCs were collected for RNA isolation, cDNA synthesis and CRTH2 qRT-PCR analysis.

Mycoplasma Test

All cell culture samples were monitored by mycoplasma test at least once a month using MycoAlert PLUS Mycoplasma Detection Kit (Lonza). 500 μL culture medium was harvested and centrifuged at 200xg for 5 minutes to eliminate cell debris. 100 μL medium was taken for 2 reactions with reagents provided in the kit. The result was determined by luminescence reading according to the protocol. All cellular samples used in this study are mycoplasma-negative.

QUANTIFICATION AND STATISTICAL ANALYSIS

Statistical significance was analyzed using Graphpad Prism Version 7.01 by one-tailed Student's t test or non-paired One-way ANOVA as reported in each figure legend. When comparing two experimental groups, unpaired Student's t test was used. When comparing multiple experimental groups, data was analyzed using one-way ANOVA, followed by Tukey's post hoc test when ANOVA has $p < 0.05$. For all test, p values were presented as $^*p < 0.05$, $^{**}p < 0.01$, and $^{***}p < 0.001$. Error bar stands for SD if not stated otherwise. Statistical details of each experiment can be found in the figure legends.

DATA AND SOFTWARE AVAILABILITY

The accession number of RNA-seq data reported in this paper is GEO: GSE116327.